



This discussion paper is/has been under review for the journal Natural Hazards and Earth System Sciences (NHESD). Please refer to the corresponding final paper in NHESD if available.

Regional-scale analysis of high-mountain multi-hazard and risk in the Pamir (Tajikistan) with GRASS GIS

F. E. Gruber and M. Mergili

Institute of Applied Geology, University of Natural Resources and Life Sciences (BOKU), Peter-Jordan-Straße 70, 1190 Vienna, Austria

Received: 11 April 2013 – Accepted: 16 April 2013 – Published: 26 April 2013

Correspondence to: M. Mergili (martin.mergili@boku.ac.at)

Published by Copernicus Publications on behalf of the European Geosciences Union.

NHESD

1, 1689–1747, 2013

Pamir regional hazard and risk analysis

F. E. Gruber and
M. Mergili

Title Page

Abstract

Introduction

Conclusions

References

Tables

Figures



Back

Close

Full Screen / Esc

Printer-friendly Version

Interactive Discussion



Abstract

We present a model framework for the regional-scale analysis of high-mountain multi-hazard and -risk, implemented with the Open Source software package GRASS GIS. This framework is applied to a 98 300 km² study area centred in the Pamir (Tajikistan). It includes (i) rock slides, (ii) ice avalanches, (iii) periglacial debris flows, and (iv) lake outburst floods. First, a hazard indication score is assigned to each relevant object (steep rock face, glacier or periglacial slope, lake). This score depends on the susceptibility and on the expected event magnitude. Second, the possible travel distances, impact areas and, consequently, impact hazard indication scores for all types of processes are computed using empirical relationships. These scores are finally superimposed with an exposure score derived from the type of land use, resulting in a raster map of risk indication scores finally discretized at the community level. The analysis results are presented and discussed at different spatial scales. The major outcome of the study, a set of comprehensive regional-scale hazard and risk indication maps, shall represent an objective basis for the prioritization of target communities for further research and risk mitigation measures.

1 Introduction

High-mountain areas are commonly experiencing pronounced environmental changes such as permafrost melting and the retreat of glaciers, caused by atmospheric temperature increase (Beniston, 2003; Huber et al., 2005; IPCC, 2007; WGMS, 2008; Harris et al., 2009). Together with earthquakes or volcanic eruptions, they disturb the dynamic equilibrium of the fragile high-mountain geomorphic systems, leading to an increased occurrence of rapid mass movements (Evans and Clague, 1994; Huggel et al., 2004a, b; Kääb et al., 2005; IPCC, 2007; Quincey et al., 2007; Harris et al., 2009; Dussailant et al., 2010; Haeberli et al., 2010a).

NHESSD

1, 1689–1747, 2013

Pamir regional hazard and risk analysis

F. E. Gruber and
M. Mergili

Title Page

Abstract

Introduction

Conclusions

References

Tables

Figures

◀

▶

◀

▶

Back

Close

Full Screen / Esc

Printer-friendly Version

Interactive Discussion

to their occurrence, are illustrated in Fig. 2. Process chains including more than one of the above process types are also considered. The study area in the Pamir (Tajikistan, Central Asia) is introduced in Sect. 2. The data used for the study is presented in Section 3 and the model framework is explained in detail in Sect. 4. Section 5 gives an overview of the model results which are discussed in Sect. 6. Section 7 summarizes the essence of the study.

2 Study area

A 98 300 km² study area in Central Asia is considered, extending from 1670 m a.s.l. near Khala-i-Khumb to 7495 m at the top of Ismoil Somoni Peak and largely corresponding to the headwaters of the Amu Darya River (Fig. 1). The northern and southern boundaries of the area are formed by the Alai and Hindukush ranges in Kyrgyzstan and Afghanistan. In between, the Pamir in the Gorno-Badakhshan Autonomous Oblast of Tajikistan represents the largest share of the study area.

The western Pamir is characterized by glacierized mountain ranges exceeding 6000 m a.s.l. and deeply incised valleys. The eastern Pamir represents an arid highland above 3500 m a.s.l. with glaciers covering only the highest peaks. The more humid northern Pamir with the Academy of Sciences and Transalai ranges peaks above 7000 m a.s.l. and is extensively glacierized. The Fedchenko Glacier extends over a length of > 75 km and covers a surface area > 700 km².

Intense tectonic uplift in combination with glacial and fluvial erosion (Mahmood et al., 2008) has resulted in a particularly pronounced relief. Consequently the geomorphic activity is high, including a large variety of mass wasting processes. They are commonly triggered by earthquakes as the seismic activity and, therefore, the seismic hazard are significant (Giardini et al., 1999). Few large historic events such as the 1911 Sarez rock slide (Schuster and Alford, 2004; Risley et al., 2006; see Fig. 2a) or the 1949 Khait rock avalanche (Evans et al., 2009b) are well documented. The deposit of the 2 km² Sarez rock slide forms the 600 m high Usoi Dam, the highest dam

Pamir regional hazard and risk analysis

F. E. Gruber and
M. Mergili

Title Page

Abstract

Introduction

Conclusions

References

Tables

Figures



Back

Close

Full Screen / Esc

Printer-friendly Version

Interactive Discussion



worldwide. It retains the 60 km long Lake Sarez, the safety of which is still disputed (e.g. Risley et al., 2006).

The climate in the study area is temperate semi-arid to arid and continental with hot summers and cold winters. Most meteorological stations in the study area have recorded a positive trend of the mean annual air temperature (MAAT) in the period 1940–2000 (Makhmadaliev et al., 2008). The state of information suffers from a lack of up-to-date high-altitude meteorological data. According to the 4th IPCC report (IPCC, 2007), the median of the projected increase of the MAAT from 1980–1999 to 2080–2099 for Tajikistan is 3.7 °C.

Consequently, many glaciers are retreating (e.g. Khromova et al., 2006; Haritashiya et al., 2009; Mergili et al., 2012a), favouring the development of lakes in the glacier forefields or in subsiding areas on the glaciers. Mergili et al. (2013) detected a total number of 652 glacial lakes in the study area. A GLOF in 2002 caused dozens of fatalities, several more lakes are susceptible to sudden drainage (Mergili and Schneider, 2011; see Fig. 2d). Further, the retreat of glaciers over steep rock cliffs (see Fig. 2b) may lead to the increased occurrence of ice avalanches. The shift of the permafrost boundary to higher areas results in the possible destabilization of rock and debris. Periglacial debris flows observed in the study area are most commonly associated with the termini of rock glaciers (see Fig. 2c).

The valleys in the study area are fairly densely populated, with Khorog as the only urban centre (see Fig. 1). The local communities strongly depend on the natural resources and are therefore affected by the consequences of the changing temperature regime in both positive and negative ways (Kassam, 2009).

3 Data

The data the high-mountain multi-risk analysis builds on are summarized in Table 1. The ASTER GDEM V2, a product of METI and NASA, is used as input digital elevation model (DEM). It is provided at a cell size of approx. 30 m × 30 m. Here a version

Pamir regional hazard and risk analysis

F. E. Gruber and
M. Mergili

Title Page

Abstract

Introduction

Conclusions

References

Tables

Figures



Back

Close

Full Screen / Esc

Printer-friendly Version

Interactive Discussion



Pamir regional hazard and risk analysis

F. E. Gruber and
M. Mergili

Title Page

Abstract

Introduction

Conclusions

References

Tables

Figures

⏪

⏩

◀

▶

Back

Close

Full Screen / Esc

Printer-friendly Version

Interactive Discussion

resampled to 60 m × 60 m is applied. Secondary data sets such as elevation with filled sinks, slope and flow direction are generated from the DEM which is further used to generate a gridded data set of the MAAT, making use of temperature data recorded at the stations of the Tajik HydroMet Agency and a vertical temperature gradient of 0.0062 °C m⁻¹ (Müllebner, 2010; Fig. 3a).

The identification of areas with melting permafrost builds on the permafrost indication map for Tajikistan presented by Mergili et al. (2012a): a set of rules-of-thumb for the lower boundaries of sporadic and discontinuous permafrost in Switzerland (Haeberli, 1975) is adapted to the conditions in Tajikistan. This set of rules is then combined with the DEM in order to produce a gridded dataset indicating the possibility of permafrost occurrence for each raster cell. Applying the temperature gradient of Müllebner (2010), the effects of atmospheric temperature increase on permafrost distribution are explored. Areas where the model predicts either sporadic or discontinuous permafrost for the current state, but no permafrost of either of the two types for a temperature increase of +2 °C or +4 °C, represent separate classes. Such areas are of particular interest for the permafrost susceptibility score S_p (Fig. 3b; see Sect. 4).

The seismic susceptibility of the area S_s is defined according to the peak ground acceleration with 10 % chance of exceedance in 50 yr (PGA), expressed in relation to gravity g . The Global Seismic Hazard Map (Giardini et al., 1999), an outcome of the Global Seismic Hazard Assessment Program (GSHAP), is employed (see Fig. 3c).

A raster map representing the glaciers in the study area is generated by a semi-automated classification of Landsat 7 satellite imagery of 2001. Three classes are distinguished: debris-covered glacier, glacier with exposed ice and no glacier (see Fig. 3c). The lakes in the study area are covered by the comprehensive lake inventory presented by Mergili et al. (2013), providing detailed information on 1640 lakes (see Table 1 and Fig. 3c). Besides the tabular information, a raster map with the unique ID of each lake is used.

The exposure of the communities in the study areas to high-mountain hazards (see Fig. 3d) is generated from a raster map depicting the land use associated with each

cell derived by the qualitative interpretation of ASTER, Landsat and Google Earth[®] imagery. Table 2 shows the key used for deriving the exposure score E from the land use map, taking values in the range 0–4. Linear structures such as roads or power lines are not considered. Each raster cell with $E > 0$ is associated to one of the 628 communities identified in the study area. The communities largely correspond to the villages depicted in the Soviet Topographic Maps 1 : 50 000 and 1 : 100 000. However, two or more villages are grouped to one community in cases where cells with $E > 0$ cannot clearly be assigned to one specific village.

4 Model

4.1 Concept of the multi-hazard and risk analysis

The high-mountain multi-hazard and -risk indication computer model is implemented with the Open Source software package GRASS GIS (Neteler and Mitasova, 2007; GRASS Development Team, 2013). This software builds on a flexible modular design. Simple bash scripting can be used to facilitate work flows by combining existing modules. Furthermore, new modules can be added by individual developers, so that the standard GIS functions are complemented by a large array of more specialized applications. Such applications can be used individually or made publicly available. Examples of mountain hazard models implemented with GRASS GIS include *r.debrisflow* (Mergili et al., 2012b), *r.avalanche* (Mergili et al., 2012c) and *r.rotstab* (Mergili et al., 2013). The model presented here builds on a combination of newly developed or upgraded modules and bash scripts. The logical framework of the model is illustrated in Fig. 4, the modules dealing with the specific process types are detailed in Sects. 4.2–4.5. The model is executed at a raster cell size of 60 m × 60 m.

The high-mountain hazard analysis procedure applied at the regional scale aims at the identification of possible (i) source areas and (ii) impact areas of hazardous processes. The risk analysis combines the hazard in the impact areas, the impact

Pamir regional hazard and risk analysis

F. E. Gruber and
M. Mergili

Title Page

Abstract

Introduction

Conclusions

References

Tables

Figures

⏪

⏩

◀

▶

Back

Close

Full Screen / Esc

Printer-friendly Version

Interactive Discussion



hazard IH , with the exposure E there in order to derive a risk indication score R in the range 0–6. Table 2 shows the matrix employed for the combination of IH and E .

The following types of processes are considered: (i) rock slides, (ii) ice avalanches, (iii) periglacial debris flows, and (iv) lake outburst floods. All of them show a potential for long travel distances and therefore represent a significant threat for the populated areas in the valleys. Even though each process type is considered separately, interactions are included in the model, such as triggering of a lake outburst flood by the impact of an upslope mass movement (see Fig. 4).

The scoring scheme employed for the hazard analysis follows the same basic principle for all types of processes. It builds on susceptibility, hazard and risk indication scores to be understood as ordinal numbers, not allowing for the use of arithmetic operations. Two-dimensional matrices are therefore used, all scores can take values in the range 0–6 (Tables 3 and 4).

The hazard indication score for the onset of a process H is computed by combining the score for the susceptibility S with the score for the expected magnitude M . The susceptibility is understood as the tendency of a lake, part of a glacier or slope to produce an event and acts as a surrogate for the frequency. The expected process magnitude is based on the possible onset volume (rock slides) or on the possible onset area (ice avalanches, lake outburst floods; see Table 3).

The impact susceptibility represents the tendency of a GIS raster cell to be affected by one of the considered processes. It is derived by routing the mass movement from the onset area down through the DEM. At the regional scale, empirical relationships are suitable for relating the travel distance L or the angle of reach ω_r of a flow to the involved volume V or the peak discharge Q_p , or for defining a global value of ω_r . The appropriate values or relationships are employed for each process type, applying the lower envelope ($\omega_{r,E}$, maximum travel distance) and the average $\omega_{r,A}$ usually observed for the considered process (see Sects. 4.2–4.5). A random walk procedure weighted for local slope and maintenance of flow direction is applied for routing. This, by applying a sufficiently large number of random walks, ensures a certain degree of lateral

Pamir regional hazard and risk analysis

F. E. Gruber and
M. Mergili

Title Page

Abstract

Introduction

Conclusions

References

Tables

Figures



Back

Close

Full Screen / Esc

Printer-friendly Version

Interactive Discussion



spreading. Furthermore, the linear distance from the starting point has to increase with each step of the routing procedure. For each passed cell, the average slope angle from the starting point, ω , is updated. Each random walk terminates as soon as $\omega \leq \omega_{r,E}$. The impact susceptibility score I of each cell builds on the maximum of the ratio

$$r_{\omega} = 1 - \frac{\tan \omega_{r,A} - \tan \omega}{\tan \omega_{r,A} - \tan \omega_{r,E}} \quad (1)$$

over all random walks. $r_{\omega} = 1$ at the average angle of reach and $r_{\omega} = 0$ at the lower envelope (see Table 4). I is determined separately for each hypothetical event. The impact hazard indication score IH map, discretized on the basis of GIS raster cells, is derived by combining H and I .

As the final step of the hazard analysis, the impact hazard indication scores IH_i for all hypothetical events i are combined in order to derive a raster map of the global hazard indication score IH . The maximum score is used for each raster cell:

$$IH = \max(IH_1, IH_2, \dots, IH_n), \quad (2)$$

where the subscripts $1, 2, \dots, n$ represent the hypothetical event IH_i is associated with, n is the total number of possible onset areas for the considered process type.

Whilst the general concept outlined is applied to all types of hazards, the specific procedures for each process type are detailed in Sects. 4.2–4.5. Below, the subscript rs stands for rock slides, ia for ice avalanches, pf for periglacial debris flows and lo for lake outburst floods. Maps of IH and R are determined separately for each process.

Given the uncertainties inherent to the regional-scale hazard and risk analysis, the discretization of the results at a raster cell size of 60 m × 60 m may pretend a level of detail not supported by the methodology used. According to the purpose of the study, the prioritization of target communities for risk mitigation measure, community-based risk indication scores for each process type (CR_{rs} , CR_{ia} , CR_{pf} , CR_{lo}) are derived. The maxima of the raster cell-based risk indication scores over all cells representing the considered village are applied. However, if the highest risk indication score R assigned

Pamir regional hazard and risk analysis

F. E. Gruber and M. Mergili

Title Page

Abstract

Introduction

Conclusions

References

Tables

Figures

⏪

⏩

◀

▶

Back

Close

Full Screen / Esc

Printer-friendly Version

Interactive Discussion



to a community applies to an area $< 10000 \text{ m}^2$, CR is reduced by 1. In such cases a lower score of R , if it applies to a larger area, may determine the score of CR for the community.

4.2 Rock slide hazard

The GRASS raster module employed for the rock slide hazard analysis is named `r.rockslide` and, to some extent, builds on the approach of Hergarten (2012). The logical framework of `r.rockslide` is illustrated in Fig. 5.

Loops over all raster cells within the study area are performed separately for four assumptions of sliding plane inclination $\beta_{s,i}$ (Table 5). If the local slope $\beta > \beta_{s,i}$ for a tested cell, the cell is considered as seed cell for a possible rock slide. In order to simulate a progressive failure, an inverse cone with a vertical axis and an inclination of $\beta_{s,i}$ is introduced. The apex of this cone coincides with the seed cell (see Fig. 5). All material above the cone surface (terrain elevation $>$ cone elevation) is considered as potential rock slide material, imitating a rock slide involving all over-steepened terrain with respect to the base cell. For each seed cell, the volume V_{rs} removed by the associated rock slide is recorded.

The susceptibility score S_{rs} for each cell with terrain elevation $>$ cone elevation is determined according to Table 5, including the sliding plane inclination $\beta_{s,i}$ and the permafrost susceptibility S_p as conditioning factors, and the seismic susceptibility S_s as possible triggering factor. S_{rs} can take values in the range 0–6. The rock slide hazard indication score H_{rs} is computed according to Table 3, with the possible event magnitude represented by the rock slide volume V_{rs} . Each cell may possibly be affected by rock slides from more than one seed cell. The final hazard indication score for each raster cell is defined as the maximum of $H_{rs,i}$ out of all relevant possible rock slides i :

$$H_{rs} = \max(H_{rs,1}, H_{rs,2}, \dots, H_{rs,n}), \quad (3)$$

where the indices $1, 2, \dots, n$ denote the id of the considered possible rock slide, n is the number of possible rock slides.

Pamir regional hazard and risk analysis

F. E. Gruber and
M. Mergili

Title Page

Abstract

Introduction

Conclusions

References

Tables

Figures

⏪

⏩

◀

▶

Back

Close

Full Screen / Esc

Printer-friendly Version

Interactive Discussion



The expected travel distance is estimated separately for each single possible slide (see Fig. 5), using a relationship of the type

$$\log_{10} \tan \omega_r = a \log_{10} V_r + b, \quad (4)$$

where ω_r is the angle of reach and V_{rs} is the rock slide volume. The curve has to be cut off at $\tan \omega = \tan \varphi$, where φ is the angle of repose. Equation (4) is only valid as long as the slide starts from rest. a and b depend on the process type, b can also be varied in order to account for uncertainties of the relationship used. Two relationships are applied:

1. For rock slides in non-glacierized areas, the prediction curve suggested by Scheidegger (1973) is used. It was derived from a set of 33 historic and prehistoric events. The correlation coefficient is 0.82, the standard deviation is 0.14298. $a = -0.15666$, $b = 0.62419$ for the average and 0.36418 for the envelope.
2. It is well established that rock slides in glacierized areas often convert into rock-ice avalanches with longer travel distances (Evans and Clague, 1988; Bottino et al., 2002). If the rock slide starts in a glacierized area, or as soon as it moves over a glacier, the relationship suggested by Noetzli et al. (2006) is applied: $a = -0.103$, $b = 0.165$ for the average and -0.040 for the envelope.

The steeper regression line for non-glacierized areas results in the prediction of longer travel distances by the Scheidegger (1973) model for very large volumes ($V_r > 361 \times 10^6 \text{ m}^3$ for the regression, $V_r > 34 \times 10^6 \text{ m}^3$ for the envelope). This phenomenon has no physical basis but can most likely be attributed to a lack of very large events in the data set used by Noetzli et al. (2006). In the r.rockslide model, the relationship yielding the longer travel distance is used for rock slides in glacierized areas. Further, the runup height R at the opposite slope is limited by the envelope of the regression derived from the dataset presented by Hewitt et al. (2008):

$$\log_{10} R \leq 0.375 \cdot \log_{10} V_r - 0.62077. \quad (5)$$

**Pamir regional
hazard and risk
analysis**

F. E. Gruber and
M. Mergili

Title Page

Abstract

Introduction

Conclusions

References

Tables

Figures

⏪

⏩

◀

▶

Back

Close

Full Screen / Esc

Printer-friendly Version

Interactive Discussion



100 random walks are performed for each rock slide or rock-ice avalanche, each of them starting at the highest raster cell of the hypothetical failure plane. The impact susceptibility score I_{rs} and the impact hazard indication score IH_{rs} are finally derived according to Eqs. (1) and (2) and Table 4. Equation (1) is here applied with the logarithms of $\tan \omega$, $\tan \omega_{r,E}$ and $\tan \omega_{r,A}$.

4.3 Ice avalanche hazard

The logical framework of the ice avalanche hazard model r.iceaval is illustrated in Fig. 6. The slope beyond which glaciers or portions of glaciers are susceptible to produce ice avalanches depends on the properties of the ice which are strongly determined by the ice temperature. As data on ice temperature is not commonly available, mean annual air temperature is often used as a surrogate. Huggel et al. (2004a) state that temperate glaciers produce ice avalanches at slopes above 25° , cold glaciers at slopes above 45° . Here, a set of 11 cases (Alean, 1985; Huggel et al., 2004a) is taken as the basis for devising a scheme for ice avalanche susceptibility S_{ia} (Fig. 7). A quadratic regression is fitted for this purpose, with

$$\tan \beta = 3.2 \times 10^{-3} \text{MAAT}^2 - 2.03 \times 10^{-2} \text{MAAT} + \eta, \quad (6)$$

where β is the slope and MAAT is the mean annual air temperature ($^\circ\text{C}$). The intercept $\eta = 0.5555$ for the regression and 0.357672 for the envelope. The thresholds applied to the ice avalanche susceptibility classes $S_{ia} = 0 - 4$ are determined from Eq. (1) with η set in the way to split the data set into quartiles (see Fig. 7). S_{ia} is increased according to the seismic susceptibility (see Table 1) so that the possible score values cover a range 0–6.

Next, clusters of cells with $S_{ia} > 0$ are identified. S_{ia} is increased by 1 for all clusters at glacier termini (no abutment). The ice avalanche hazard indication score H_{ia} is derived according to Table 3, combining S_{ia} and the area of each cluster.

For each cluster, 100 random walks are applied for routing the possible ice avalanche down, starting at the highest point of the cluster. According to Huggel et al. (2004a),

Pamir regional hazard and risk analysis

F. E. Gruber and
M. Mergili

Title Page

Abstract

Introduction

Conclusions

References

Tables

Figures

⏪

⏩

◀

▶

Back

Close

Full Screen / Esc

Printer-friendly Version

Interactive Discussion



Pamir regional hazard and risk analysis

F. E. Gruber and
M. Mergili

Title Page

Abstract

Introduction

Conclusions

References

Tables

Figures

⏪

⏩

◀

▶

Back

Close

Full Screen / Esc

Printer-friendly Version

Interactive Discussion

the travel path of ice avalanches is constrained by an average slope of 17° , except for very large events ($> 5 \times 10^6 \text{ m}^3$). However, such events are most commonly rock-ice avalanches or complex process chains (e.g. 1962 and 1970 Huascarán events, 2002 Kolka/Karmadon event), which are covered separately here, or related to volcanic processes (1980 Iliamna event, Alaska). Therefore, and since the ice avalanche volume cannot be derived with the method applied, we constrain the impact area with an average slope of 17° ($\tan \omega_{r,E} = 0.31$). In the dataset used by Huggel et al. (2004a), the minimum value of the average slope is $\tan \omega = 0.44$, $\tan \omega_{r,E}$ is set to the average 0.375 and I_{ia} is computed according to Eq. (1). Equation (2) and Table 4 are applied in order to derive the ice avalanche impact hazard indication score IH_{ia} .

4.4 Periglacial debris flow hazard

Melting permafrost on steep slopes leaves behind a certain amount of loose debris susceptible to mobilization as debris flows. Such processes may occur in the active layer, but even more where permafrost is retreating. Here, we only consider areas where retreating permafrost is assumed (see Table 1; Mergili et al., 2012a). Figure 8 shows the logical frame work of the periglacial debris flow model r.periflow. Huggel et al. (2004b) noted that, in contrast to ordinary debris flows, parameters such as slope curvature or the proximity to the stream network are hardly significant for the onset of such processes. Further, they commonly occur at slope angles from 27° to 38° . Table 6 shows the scheme applied here for deriving the susceptibility of each raster cell to periglacial debris flows S_{pf} in the range from 0 to 6. We follow the findings of Huggel et al. (2004b) with regard to slope. Unfortunately, no means for the reliable distinction of bedrock and debris at the relevant scale are known to the authors. Besides slope and the state of the permafrost, the seismic susceptibility is considered for deriving S_{pf} (see Tables 1 and 6).

In contrast to the other processes considered in the present study, there are no means to approximate the onset volume and therefore the process magnitude. Clusters of susceptible cells are often large whilst the onset of debris flow processes is most

commonly a rather localized process. We therefore use the approximation $H_{pf} = S_{pf}$ (see Fig. 8).

Consequently, the routing procedure (i) has to be started separately from each raster cell with $S_{pf} > 0$ and (ii) the average slope determining the impact area has to be independent from volume. Due to the commonly large clusters of starting cells, only 10 random walks are started from each cell. Huggel et al. (2004b) give an envelope average slope of the travel path of 11° ($\tan \omega_{r,E} = 0.194$) which is also applied here. The maximum average slope is taken from Corominas et al. (2003) who provide a value of 26° ($\tan \omega = 0.488$) for debris flows $< 800 \text{ m}^3$ propagating on undisturbed flow paths assumed for the study area. The average of the two values, 0.341, is taken as $\tan \omega_{r,A}$. I_{pf} is computed according to Eq. (1). For $I_{pf} < 4$, the runup on the opposite slope is restricted. Equation(2) and Table 4 are applied to derive the periglacial debris flow impact hazard indication score IH_{pf} .

4.5 Lake outburst hazard

An improved version of the GRASS GIS raster module r.glof (Mergili and Schneider, 2011) is used for the lake outburst hazard analysis. The logical framework of r.glof is illustrated in Fig. 9.

First, the susceptibility scores for (i) lake outburst caused by internal factors (dam failure) $S_{lo,i}$ and (ii) lake outburst triggered by external factors (impact of mass movements) $S_{lo,e}$ are considered separately (see Fig. 9). $S_{lo,i}$ and $S_{lo,e}$ can take values in the range 0–6, negative values are set to 0.

The derivation of $S_{lo,i}$ builds on the following key parameters: (i) lake type, indicating the dam material; (ii) mode of lake drainage; (iii) lake evolution; (iv) dam geometry; (v) permafrost susceptibility; (vi) seismic susceptibility (see Table 1). Table 7 shows the scoring scheme applied. The lake type (Mergili et al., 2013) is taken as basis, with glacial lakes receiving the highest score. Dams with seepage are considered more susceptible to failure than dams with surface runoff, and growing lakes are considered more susceptible than stable or shrinking ones. The dam geometry is expressed as

Pamir regional hazard and risk analysis

F. E. Gruber and
M. Mergili

Title Page

Abstract

Introduction

Conclusions

References

Tables

Figures



Back

Close

Full Screen / Esc

Printer-friendly Version

Interactive Discussion



an idealized average downstream slope of the dam: the dam width W is defined as the Euclidean distance between the lake outlet and the closest raster cell along the downstream flow path with a lower elevation than the average lake bottom, using the average lake depth D_l according to Huggel et al. (2002):

$$D_l = 1.04 \times 10^{-1} A_l^{0.42}, \quad (7)$$

where A_l is the lake area (m^2), D_l is given in m. The tangent of the average slope of the dam in outflow direction, $\tan \beta_d$, is derived as D_l/W . For very gentle downstream average slopes $\tan \beta_d < 0.02$, $S_{lo,i}$ is decreased by 1 (see Table 7).

The event at Laguna 513 in the Cordillera Blanca (Haeberli et al., 2010b) has shown the need to include the entire catchment when analyzing lake outburst susceptibility. The topographic susceptibility TS is introduced in order to account for this need, employing the impact hazard indication scores for rock slides IH_{rs} , for ice avalanches IH_{ia} , for periglacial debris flows IH_{pf} , and for outburst floods of lakes in the upper catchment IH_{lo} . The overall maximum score over the raster cells representing the considered lake ($IH_{ia,max}$, $IH_{rs,max}$, $IH_{pf,max}$, and $IH_{lo,max}$) applies, but the impact of periglacial debris flows and upstream lake outburst floods is down-weighted:

$$TS = \max (IH_{rs,max}, IH_{ia,max}, IH_{pf,max} - 3, IH_{lo,max} - 3). \quad (8)$$

The topographic susceptibility is taken as the basis for the rating of the susceptibility to lake outburst triggered by external factors $S_{lo,e}$. If direct calving of ice into the lake is possible, the score for $S_{lo,e}$ is set to a minimum of 3.

The maximum of $S_{lo,i}$ and $S_{lo,e}$ is used as lake outburst susceptibility S_{lo} . S_{lo} is reduced for lakes with a high freeboard F (defined as the difference between the DEM with filled sinks and the original DEM for the lake centre): for lakes with $F > 50$ m the score is decreased by 3. For lakes with $F > 25$ m it is decreased by 2, and for lakes with $F > 10$ m, the score is decreased by 1 in order to derive the final value of S_{lo} .

The lake area is most likely the best surrogate for M_{lo} since the lake volume is uncertain. Table 7 shows the matrix for the lake outburst hazard indication score H_{lo} which is discretized on the basis of lakes.

**Pamir regional
hazard and risk
analysis**

F. E. Gruber and
M. Mergili

Title Page

Abstract

Introduction

Conclusions

References

Tables

Figures

⏪

⏩

◀

▶

Back

Close

Full Screen / Esc

Printer-friendly Version

Interactive Discussion



Pamir regional hazard and risk analysis

F. E. Gruber and
M. Mergili

Title Page

Abstract

Introduction

Conclusions

References

Tables

Figures

⏪

⏩

◀

▶

Back

Close

Full Screen / Esc

Printer-friendly Version

Interactive Discussion

Possible outburst floods are routed downwards through the DEM separately for each lake, the travel distance is determined according to the relationships listed in Table 8. After the deposition of the debris or mud, or if not much sediment is entrained at all, the flood may propagate much farther: Haeberli (1983) suggests an average angle of reach of $2 - 3^\circ$, but also travel distances exceeding 200 km are reported (e.g. Hewitt, 1982).

In order to achieve a robust estimate of the travel distance, the impact area of possible lake outburst floods and, consequently, the impact susceptibility I_{lo} , the approaches T1–T4 shown in Table 8 are combined (Eq. 1 is not applied for lake outburst floods). The lake outburst flood is routed down starting from the outlet of the considered lake. 800 random walks are performed for each lake. A random walk is forced to terminate if it impacts a larger lake.

For T1, the debris flow volume V_d is set to five times the outburst volume (maximum sediment concentration in steep flow channels $\sim 80\%$ according to Iverson, 1997) in order to account for sediment bulking. The outburst volume is set to the entire lake volume, lake area A_l multiplied with lake depth D_l). For T2, we use an angle of reach $\omega_r = 8^\circ$ which is most likely more suitable for the study area (Mergili and Schneider, 2011) than $\omega_r = 11^\circ$ as suggested by Haeberli (1983). Several authors have introduced empirical relationships for relating the peak discharge Q_p ($\text{m}^3 \text{s}^{-1}$) – required as input for the relationship T3 in Table 8 – to the outburst volume and the dam height (Costa, 1985; Costa and Schuster, 1988; Walder and O'Connor, 1997; Table 9). Q_p is determined from the maximum of the results computed with the relationships Q1–Q6 shown in Table 9. T1 and T3 are only applied to glacial lakes as there is no basis available for calculating the depth or volume of lakes assigned to the other types. Instead, the angle of reach is set to $\omega_r = 11^\circ$ (the value suggested by Haeberli, 1983) for T1 and to $\omega_r = 14^\circ$ for T3.

The number of relationships T1–T4 (see Table 8) predicting an impact on a given raster cell determines the impact susceptibility: if all four relationships predict an impact, $I_{lo} = 6$, three relationships results in $I_{lo} = 5$ and so forth. For $I_{lo} < 6$, the runoff on

the opposite slope is restricted. If only an impact as flood is predicted, (T_4 ; $I_{10} \leq 3$), the impact susceptibility is further differentiated according to ω : for $\omega \geq 6$, $I_{10} = 3$, for $\omega \geq 4$, $I_{10} = 2$ and for $\omega \geq 2$, $I_{10} = 1$. T_4 is only applied to lakes $\geq 50\,000\text{ m}^2$. Furthermore, the criterion that the distance from the source has to increase with each computing step is disabled for floods.

In an analogous way to the scores for the rock slides, ice avalanches and periglacial debris flows (see Sections 4.2–4.4), the impact hazard indication score is then derived by combining I_{10} with H_{10} of the corresponding lake (see Table 4). The global impact hazard indication score IH_{10} of a given raster cell is defined as the maximum of all lake-specific scores (see Eq. 2).

5 Results

The total area with significant periglacial debris flow (PF) susceptibility/hazard is much larger than those for the other hazard types: 9.9% of the entire study area are designated as possible PF source areas, based on the criteria defined in Table 6. 42.7% out of this area are assigned the three higher susceptibility scores 4–6 (Fig. 10a). This pattern indicates the ubiquity of hazardous areas on the one hand, but also the limited means of a sharper delineation on the other hand. In contrast, the ice avalanche (IA) susceptibility and the lake outburst (LO) susceptibility, due to their confinement to glaciers and lakes, respectively, are constrained in a much sharper way. 1.6% of the total study area are identified as susceptible to IA, 64.5% out of this area are assigned the susceptibility scores 4–6 (see Fig. 10a). The LO susceptibility is discretized on the basis of lakes. 70.9% of all lakes are assigned susceptibility scores > 0 , 50.0% of these lakes the susceptibility scores 4–6 (see Fig. 10a). The rock slide (RS) susceptibility displays intermediate patterns in terms of the total area identified as susceptible (4.7% of the total study area). However, only 16.2% of this area – a much lower value than those associated with the other process types – are assigned the susceptibility

Pamir regional hazard and risk analysis

F. E. Gruber and
M. Mergili

Title Page

Abstract

Introduction

Conclusions

References

Tables

Figures

⏪

⏩

◀

▶

Back

Close

Full Screen / Esc

Printer-friendly Version

Interactive Discussion

scores 4–6 (see Fig. 10a). The reason for this phenomenon is the limited area occupied by very steep slopes (see Table 5).

The distribution of the raster cells or lakes identified as susceptible among the six hazard indication score classes is illustrated in Fig. 10b, depending on the susceptibility and the possible process magnitude (see Table 3). 38.1 % of the RS and 68.4 % of the IA are assigned the hazard indication scores 4–6. In the case of PF, hazard and susceptibility are identical due to lacking means for an estimation of the magnitude (see Sect. 4.4). Comparatively few lakes (23.9 %) are assigned the LO hazard indication scores 4–6. This phenomenon is explained by the large number of rather small but highly susceptible lakes.

Figure 11 represents the hazard indication scores for each process type broken down to the level of small catchments identical to the output parameter basin of the GRASS GIS raster module `r.watershed` (GRASS Development Team, 2013) with a threshold parameter of 5000. The maximum out of all raster cell-based hazard indication scores is shown for each catchment, except for the LO hazard where the value assigned to each lake is illustrated.

As expected, the RS hazard (see Fig. 11a) is highest in areas with a particularly steep topography in the northern and central Pamir. More localized high-hazard areas are distributed throughout the study area. The IA hazard (see Fig. 11b) is high in most glacierized areas (see Fig. 3d), particularly in parts of the northern Pamir where large portions of steep glaciers are extremely abundant. Within these zones the inter-catchment differentiation of hazardous areas is rather poor.

The PF hazard is poorly differentiated at the catchment scale: steep slopes near the permafrost boundary are almost ubiquitous in the study area (see Fig. 3b), except for the elevated and comparatively gently inclined south eastern portion. The most notable regional pattern is therefore attributed to the seismic susceptibility. The patterns observed in Fig. 11c are further a consequence of the limited input information that can be reasonably applied at the regional scale (see Table 6). A detailed inventory of rock glaciers (comparable to the inventories prepared for glaciers and lakes, see Fig. 3d)

Pamir regional hazard and risk analysis

F. E. Gruber and
M. Mergili

Title Page

Abstract

Introduction

Conclusions

References

Tables

Figures



Back

Close

Full Screen / Esc

Printer-friendly Version

Interactive Discussion



could help to sharpen the distinction between more and less hazardous areas. However, as rock glaciers are extremely common throughout the study area, the patterns at the inter-catchment level would most likely remain unchanged.

As the LO hazard is directly related to the well-known lake distribution it can be discretized at a high level of detail (see Fig. 11d). Nine lakes are assigned the highest LO hazard indication score $H_{lo} = 6$, the largest of them is Lake Sarez. Even though – or because – the safety of Lake Sarez is highly disputed (e.g. Risley et al., 2006), this classification seems reasonable. The LO susceptibility score $S_{lo} = 5$ is a consequence of the high topographic susceptibility. The same is true for Lake Zardiv, with 0.7 km² the second largest lakes with $H_{lo} = 6$ (see Fig. 11d). Further lakes of interest are, e.g. Lake Khavraz and Lake Shiva. Lake Khavraz is an 1.9 km² lake impounded behind a rock glacier at an elevation of 4000 m a.s.l., in the zone of possibly melting permafrost. Here both the topographic susceptibility ($S_{lo,e} = 5$) and the LO susceptibility due to internal factors ($S_{lo,i} = 5$) are at high levels. Lake Shiva is assigned a susceptibility in the medium range of the scale ($S_{lo} = 3$) and a sudden drainage is not likely but, due to the large size of 15.2 km², $H_{lo} = 5$. The lake is located close to several communities in the Panj Valley which could be affected in the case of such an event. The largest lake in the study area, Kara Kul, is assigned a hazard indication score of 4 (see Fig. 11d). The LO susceptibility of Kara Kul is rated with a score of $S_{lo} = 2$, only the very large lake area (405 km²) leads to the relatively high hazard indication score. The fact that a closer look reveals no significant outburst hazard of Kara Kul suggests that the approach used tends to overestimate the hazard for large lakes. One reason for this phenomenon is the topographic susceptibility: large lakes have the ability to alleviate the impact of mass movements rather than small lakes. However, an objective basis to include the dependence of the topographic susceptibility on lake size is missing. Table 10 summarizes the LO susceptibility and hazard by lake type. Whilst – as prescribed by the scheme shown in Table 7 – glacial lakes clearly display the higher scores of the LO susceptibility due to internal factors, this tendency is less pronounced – but still visible – for the LO susceptibility due to external factors.

**Pamir regional
hazard and risk
analysis**F. E. Gruber and
M. Mergili

Title Page

Abstract

Introduction

Conclusions

References

Tables

Figures

◀

▶

◀

▶

Back

Close

Full Screen / Esc

Printer-friendly Version

Interactive Discussion



Pamir regional hazard and risk analysis

F. E. Gruber and
M. Mergili

Title Page

Abstract

Introduction

Conclusions

References

Tables

Figures

⏪

⏩

◀

▶

Back

Close

Full Screen / Esc

Printer-friendly Version

Interactive Discussion

The median and maximum travel distances computed for each process type are summarized in Table 11. The RS model commonly predicts travel distances of 3.0 km (average)–5.6 km (envelope), but for very large events ($> 800 \times 10^6 \text{ m}^3$) extending over vertical distances $> 4000 \text{ m}$ the model, when applied with the envelope, predicts a travel distance of almost 50 km (see Eq. 4). The IA model ($\omega_{r,E} = 17^\circ$) and the PF model ($\omega_{r,E} = 11^\circ$) predict shorter travel distances. Note that, in both cases, the difference between the median and the maximum is only caused by topography and not by the assumed process magnitude. The LO model predicts the possibility of a significant debris flow for less than half of all lakes (no meaningful median value can therefore be given in Table 11). The reason for this phenomenon is mainly the gentle slope observed downstream from many lakes. However, lakes with steeper downstream slopes can produce debris flows with travel distances $> 15 \text{ km}$ and floods $> 80 \text{ km}$, according to the model.

Figure 12 shows the distribution of the impact hazard. For clarity, only the raster cell values along the main flow channels are shown. It is clear that the general patterns of the impact hazard at the broad scale resemble those of the hazard shown in Fig. 11: whilst a possible impact of rock slides and periglacial debris flows is shown for most valleys particularly in the western part of the study area (Figs. 12a and 12c), a more localized impact of ice avalanches and lake outburst floods is suggested by the model (Figs. 12b and 12d).

The distribution of community risk over the study area reflects the patterns shown in Figs. 11 and 12 on the one hand, and the distribution of the exposed communities on the other hand. Figure 13 illustrates the relative frequency of the community risk indication score classes for 15 regions within the study area, each of them representing a catchment or section of a catchment. The eastern Pamir is considered as one single region due to the low number of communities there. Except for the very western part of the study area, the eastern Pamir and the Kyrgyz part of the study area (Chan-Alai Valley) in the north, all regions are dominated by communities with a significant rock slide risk, the highest scores are observed for the villages in the rugged Bartang and

Pamir regional hazard and risk analysis

F. E. Gruber and
M. Mergili

Title Page

Abstract

Introduction

Conclusions

References

Tables

Figures



Back

Close

Full Screen / Esc

Printer-friendly Version

Interactive Discussion



middle Panj valleys as well as in the Gunt Valley (see Fig. 13a). The hot spots of ice avalanche risk are identified in the Vanch and Bartang valleys, both deeply incised into glacierized mountain ranges (see Fig. 13b). This type of risk plays a less prominent role in the other regions. Also the risk of periglacial debris flows is highest in the deep gorges of the western Pamir, decreasing towards north where permafrost is less abundant (see Fig. 13c). However, the model predicts a significant PF risk for most communities throughout the study area. This is not the case for the risk caused by lake outburst floods, which is significant mainly in the south western Pamir and in part of the northern Pamir (see Fig. 13d). The LO community risk indication score $CR_{10} = 6$ is not assigned to any village. Table 12 summarizes the relative frequency of villages assigned to each class with respect to all four hazard types.

A composite hazard and risk indication map is prepared for the entire study area. It provides a visual overlay of the hazard, impact hazard and community-based risk indication scores for each of the four process types considered in the study. Figure 14 shows this map for a selected area covering the Gunt Valley and its tributaries (see Fig. 1 for delineation). The area affected by the prehistoric Charthem rock slide (see Fig. 14a) is very well reproduced by the model, therefore a high RS risk is assigned to the nearby communities. However, also several other communities and lakes are possibly impacted by rock slides. The patterns of IA hazard and risk illustrate the isolated appearance of this type of hazard in the area (see Fig. 14b). Even though the main effect of the process is the possible impact on lakes, some communities in the main valley are at risk, but assigned rather low scores. Areas of PF hazard (see Fig. 14c) are strictly confined to steep slopes near the permafrost boundary which are however very common along the slopes of most valleys, confirming the broad-scale patterns shown in Fig. 11c. Therefore, most of the communities in the valleys are identified as at risk. The occurrence of periglacial debris flows in this area, often starting from the termini of rock glaciers, is evident in the field and from remotely sensed imagery (see Fig. 2c). The associated debris cones are located in zones of high impact hazard identified by the model. In contrast, most lakes are located where permafrost is assumed stable.

Pamir regional hazard and risk analysis

F. E. Gruber and
M. Mergili

Title Page

Abstract

Introduction

Conclusions

References

Tables

Figures

⏪

⏩

◀

▶

Back

Close

Full Screen / Esc

Printer-friendly Version

Interactive Discussion

Several lakes have developed near the termini of the glaciers of the tributary valleys (Mergili and Schneider, 2011; Mergili et al., 2013). Three of them are assigned the hazard indication score $H_{I_o} = 5$ (see Fig. 14d). The debris flow travel distances predicted by the LO model are relatively short, only debris flows from two lakes could reach the communities of the main valley: the village of Varshedz is just located at the terminus of a possible debris flow starting from Lake Varshedz (see Fig. 2d; lake area 0.16 km^2 , $S_{I_o} = 5$, $H_{I_o} = 5$). Lake Nimats, an erosion lake with $S_{I_o} = 4$ and $H_{I_o} = 5$, drains into a very steep channel heading directly down to the main valley. In the case of a (not very likely) sudden drainage, the nearby villages would most likely suffer substantial damage. The impact area of the distal floods resulting from the possible drainage of Lake Varshedz or Lake Nimats is characterized by lower to medium community risk indication scores of the possibly affected villages. The largest lake shown in Fig. 14d is Rivakkul (1.2 km^2 , $S_{I_o} = 4$, $H_{I_o} = 5$). It is characterized by a very gently inclined downstream valley. As a result, the model predicts only a comparatively short travel distance of a possible outburst flood (4.6 km), being alleviated far upslope from the villages in the main valley.

6 Discussion

The purpose of the model approach introduced in the previous sections and the resulting hazard and risk indication maps is to provide a reproducible basis for targeted hazard and risk assessment studies and mitigation measures at the community scale. The approach chosen is thought to be useful for the study area in the Pamir for two reasons.

First, the general difficulty of establishing frequencies for rare or singular events in combination with sparse historical data in the study area makes strictly quantitative approaches such as statistical methods inapplicable. Therefore a hazard and risk indication scoring scheme has to be applied, even though such a concept introduces a certain degree of subjectivity.

Pamir regional hazard and risk analysis

F. E. Gruber and
M. Mergili

Title Page

Abstract

Introduction

Conclusions

References

Tables

Figures

⏪

⏩

◀

▶

Back

Close

Full Screen / Esc

Printer-friendly Version

Interactive Discussion

predicted conditions and scenarios are likely to be realistic, uncertainties are hard to quantify. The seismic hazard map used (Giardini et al., 1999) is a highly generalized global dataset. Other essential information such as the distinction bedrock – residual rock or the orientation and dip of the bedding planes of geological layers are hardly manageable at the scale relevant for a study of this type.

The scoring schemes used (see Tables 2–7) are founded on expert knowledge. The interpretation of the model results have to consider the characteristics of the scheme used for each process. Necessarily, the schemes contain \pm arbitrary thresholds such as those used for the event magnitude (see Table 3) or the 45° minimum slope for rock slides already used earlier by Hergarten (2012).

The modelling of the travel distance and the impact area of the considered processes is derived from the statistics of observed events. These statistics are reasonably robust for rock slides and rock ice avalanches (Scheidegger, 1973; Evans and Clague, 1988; Bottino et al., 2002; Noetzli et al., 2006) and also for ice avalanches (Huggel et al., 2004a). However, they are based on observations from other mountain areas such as the Alps. Their application is based on the hypothesis that (i) the patterns observed there are comparable to those in the Pamir and (ii) that the – often rather small – datasets used for the derivation of the patterns and thresholds cover a representative sample of the reality. This is equally true for the slope-temperature curve shown in Fig. 7. The situation is even more difficult for periglacial debris flows (Huggel et al., 2004a) and particularly for lake outburst floods. The threshold of $\omega_{r,E} = 11^\circ$ used by Huggel et al. (2004a, b) for debris flows from lake outburst events is not applicable to the Pamir as the 2002 Dasht event, where $\omega_{r,E} \sim 9.3^\circ$, has shown (Mergili and Schneider, 2011). Also the parameterization of floods developing from lake outburst events is nothing more than a rough estimate so that the results (such as the short travel distance predicted for a sudden drainage of Rivakkul, see Fig. 14d) have to be interpreted with utmost care.

Further, the application of average slopes neglects the loss of energy due to changes of the flow direction. Strictly spoken, such concepts should only be used for straight flow

paths. The criterion that the motion has to move away from the source with each step of the random walk partly accounts for this limitation.

Possible impact wave due to mass movements into lakes are explicitly accounted for by the model. Other types of interactions are included indirectly: the conversion of rock slides into rock-ice avalanches by the impact on glaciers is implicitly considered in the rock slide model, even though there are no means to estimate the entrainment of snow or ice. In the case of rock slides and rock-ice avalanches, the empirical relationships used implicitly include cascading effects such as the conversion into debris flows. Some process interactions are out of scope of the present study, such as the damming of lakes by mass movements and possible subsequent drainage. The same is true for the entrainment of debris, modelling of which remains a challenge particularly at the scale of the present study.

The approach used does not allow for an analytical overlay of the susceptibility, hazard, impact hazard and risk indication scores associated to each process type. Even though attempted as far as possible, a homogenization of the scoring schemes for the different processes proves highly problematic due to the missing physical basis. The data the analysis is based on differs between the processes: e.g. the possible magnitude of rock slides is given in maximum volumes whilst only the maximum involved surface area allowed under the assumptions taken is used for possible ice avalanches and lake outburst floods (see Table 3). Also the schemes for susceptibility can hardly be homogenized (see Tables 5–7; Fig. 7), partly due to the varying level of detail of the available input data.

7 Conclusions

A regional-scale multi-hazard and -risk indication model was introduced, including four selected high-mountain processes: (i) rock slides and rock avalanches, (ii) ice-avalanches, (iii) periglacial debris flows, and (iv) lake outburst floods. The model results for a very large area centred in the Pamir (Tajikistan) were presented and discussed.

Pamir regional hazard and risk analysis

F. E. Gruber and
M. Mergili

Title Page

Abstract

Introduction

Conclusions

References

Tables

Figures



Back

Close

Full Screen / Esc

Printer-friendly Version

Interactive Discussion



Pamir regional hazard and risk analysis

F. E. Gruber and
M. Mergili

Title Page

Abstract

Introduction

Conclusions

References

Tables

Figures

⏪

⏩

◀

▶

Back

Close

Full Screen / Esc

Printer-friendly Version

Interactive Discussion

The model shall help to distinguish areas with higher from those with lower risk, even though the possibilities for comparison with observed events are limited. The interpretation of the model results – preferably at the level of communities, catchments or regions – has to take into account the characteristics of the scoring schemes as well as the limitations of the input data and the methodology used.

Acknowledgements. The work presented is part of the project PAMIR supported by the European Commission (EC) and the Austrian Development Agency (ADA), as well as of the project TajHaz supported by FOCUS Humanitarian Assistance (an affiliate of the Aga Khan Development Network), the Swiss Agency for Development and Cooperation (SDC) and the UK Department for International Development (DFID). The Tajik Agency of Hydrometeorology has provided meteorological data. Special thanks for their support go to Matthias Benedikt, Johannes P. Müller and Jean F. Schneider, BOKU University, Vienna.

References

- Alean, J.: Ice avalanches: some empirical information about their formation and reach, *J. Glaciol.*, 31, 324–333, 1985.
- Beniston, M.: Climatic Change in Mountain Regions: A Review of Possible Impacts, *Clim. Change*, 59, 5–31, doi:10.1023/A:1024458411589, 2003.
- Bolch, T., Peters, J., Yegorov, A., Prafhan, B., Buchroithner, M., and Blagoveshchensky, V.: Identification of potentially dangerous glacial lakes in the northern Tien Shan, *Nat. Hazards*, 59, 1691–1714, doi:10.1007/s11069-011-9860-2, 2011.
- Bottino, G., Chiarle, M., Joly, A., and Mortara, G.: Modelling Rock Avalanches and Their Relation To Permafrost Degradation in Glacial Environments. *Permafrost Periglac.*, 13, 283–288, doi:10.1002/ppp.432, 2002.
- Breien, H., DeBlasio, F. V., Elverhoi, A., and Hoeg, K.: Erosion and morphology of a debris flow caused by a glacial lake outburst flood, Western Norway, *Landslides*, 5, 271–280, doi:10.1007/s10346-008-0118-3, 2008.
- Carey, M.: Living and dying with glaciers: people’s historical vulnerability to avalanches and outburst floods in Peru, *Global Planet. Change*, 47, 122–134, doi:10.1016/j.gloplacha.2004.10.007, 2005.

Pamir regional hazard and risk analysis

F. E. Gruber and
M. Mergili

Title Page

Abstract

Introduction

Conclusions

References

Tables

Figures

◀

▶

◀

▶

Back

Close

Full Screen / Esc

Printer-friendly Version

Interactive Discussion

- Cenderelli, D. A. and Wohl, E. E.: Peak discharge estimates of glacial lake outburst floods and “normal” climatic floods in Mount Everest region, Nepal, *Geomorphology*, 40, 57–90, doi:10.1016/S0169-555X(01)00037-X, 2001.
- Clarke, G. K. C.: Glacier outburst floods from “Hazard Lake”, Yukon Territory, and the problem of flood magnitude prediction, *J. Glaciol.*, 28, 3–21, 1982.
- Corominas, J., Copons, R., Vilaplana, J. M., Altamir, J., and Amigó, J.: Integrated Landslide Susceptibility Analysis and Hazard Assessment in the Principality of Andorra, *Nat. Hazards*, 30, 421–435, doi:10.1023/B:NHAZ.0000007094.74878.d3, 2003.
- Costa, J. E.: Floods from Dam Failures, Denver, Colorado, U.S. Geol. Surv. Open File Rep. 85-560, 54 pp., 1985.
- Costa, J. E. and Schuster, R. L.: The formation and failure of natural dams, *Geol. Soc. Am. Bull.*, 100, 1054–1068, doi:10.1130/0016-7606(1988)100<1054:TFAFON>2.3.CO;2, 1988.
- Dussaillant, A., Benito, G., Buytaert, W., Carling, P., Meier, C., and Espinoza, F.: Repeated glacial-lake outburst floods in Patagonia: an increasing hazard?, *Nat. Hazards*, 54, 469–481, doi:10.1007/s11069-009-9479-8, 2010.
- Evans, S. G.: The maximum discharge of outburst floods caused by the breaching of man-made and natural dams, *Can. Geotech. J.*, 23, 385–387, doi:10.1139/t86-053, 1986.
- Evans, S. G. and Clague, J. J.: Catastrophic rock avalanches in glacial environments, in: *Landslides*, edited by: Bonnard, C., A.A. Balkema, Rotterdam, 2, 1153–1158, 1988.
- Evans, S. G. and Clague, J. J.: Recent climatic change and catastrophic geomorphic processes in mountain environments, *Geomorphology*, 10, 107–128, doi:10.1016/0169-555X(94)90011-6, 1994.
- Evans, S. G., Bishop, N. F., Fidel Smoll, L., Valderrama Murillo, P., Delaney, K. B., and Oliver-Smith, A.: A re-examination of the mechanism and human impact of catastrophic mass flows originating on Nevado Huascarán, Cordillera Blanca, Peru in 1962 and 1970, *Eng. Geol.*, 108, 96–118, doi:10.1016/j.enggeo.2009.06.020, 2009a.
- Evans, S. G., Roberts, N. J., Ischuk, A., Delaney, K. B., Morozova, G. S., and Tutubalina, O.: Landslides triggered by the 1949 Khatit earthquake, Tajikistan, and associated loss of life, *Eng. Geol.*, 109, 195–212, doi:10.1016/j.enggeo.2009.08.007, 2009b.
- Giardini, D., Grünthal, G., Shedlock, K., and Zhang, P.: The GSHAP Global Seismic Hazard Map, *Ann. Geophys.*, 42, 6 pp., doi:10.4401/ag-3784, 1999.

GRASS Development Team: Geographic Resources Analysis Support System (GRASS) Software. Open Source Geospatial Foundation Project, available at: <http://grass.osgeo.org> (last access: 19 April 2013), 2013.

Haerberli, W.: Untersuchungen zur Verbreitung von Permafrost zwischen Flüelapass und Piz Grialetsch (Graubünden), Dissertation, University of Basel, Switzerland, 1975 (in German).

Haerberli, W.: Frequency and characteristics of glacier floods in the Swiss Alps, *Ann. Glaciol.*, 4, 85–90, 1983.

Haerberli, W., Clague, J. J., Huggel, C., and Kääh, A.: Hazards from lakes in high-mountain glacier and permafrost regions: Climate change effects and process interactions, in: *Avances de la Geomorfología en España, 2008-2010*, edited by: Úbeda, X., Vericat, D., and Batalla, R. J., XI Reunión Nacional de Geomorfología, Solsona, Spain, 439–446, 2010a.

Haerberli, W., Portocarrero, C., and Evans, S.: Nevado Hualcán, Laguna 513 y Carhuaz 2010 – Observaciones, evaluación y recomendaciones (un corto informe técnico luego de las reuniones y visita de campo en Julio 2010), unpublished report on behalf of the Comunidad Provincial de Carhuaz, 2010b (in Spanish).

Haritashya, U. K., Bishop, M. P., Shroder, J. F., Bush, A. B. G., and Bulley, H. N. N.: Space-based assessment of glacier fluctuations in the Wakhan Pamir, Afghanistan, *Climatic Change*, 94, 5–18, doi:10.1007/s10584-009-9555-9, 2009.

Harris, C., Arenson, L. U., Christiansen, H. H., Etzelmüller, B., Frauenfelder, R., Gruber, S., Haerberli, W., Hauck, C., Hölzle, M., Humlum, O., Isaksen, K., Kääh, A., Kern-Lütschg, M. A., Lehning, M., Matsuoka, N., Murton, J. B., Nötzli, J., Phillips, M., Ross, N., Seppälä, M., Springman, S. M., and VonderMühl, D.: Permafrost and climate in Europe: Monitoring and modelling thermal, geomorphological and geotechnical responses, *Earth-Sci. Rev.*, 92, 117–171, doi:10.1016/j.earscirev.2008.12.002, 2009.

Harrison, S., Glasser, N., Winchester, V., Haresign, E., Warren, C., and Jansson, K.: A glacial lake outburst flood associated with recent mountain glacier retreat, *Patagonian Andes, Holocene*, 16, 611–620, doi:10.1191/0959683606hl957rr, 2006.

Hergarten, S.: Topography-based modelling of large rockfalls and application to hazard assessment, *Geophys. Res. Lett.*, 39, L13402, doi:10.1029/2012GL052090, 2012.

Hewitt, K.: Natural dams and outburst floods in the Karakorum Himalaya, in: *Hydrological aspects of alpine and high-mountain areas*, edited by: Glen, J. W., IAHS Publication, 138, 259–269, 1982.

NHESSD

1, 1689–1747, 2013

Pamir regional hazard and risk analysis

F. E. Gruber and
M. Mergili

Title Page

Abstract

Introduction

Conclusions

References

Tables

Figures

◀

▶

◀

▶

Back

Close

Full Screen / Esc

Printer-friendly Version

Interactive Discussion

**Pamir regional
hazard and risk
analysis**F. E. Gruber and
M. Mergili

Title Page

Abstract

Introduction

Conclusions

References

Tables

Figures

⏪

⏩

◀

▶

Back

Close

Full Screen / Esc

Printer-friendly Version

Interactive Discussion

Hewitt, K. and Liu, J.: Ice-dammed lakes and outburst floods, Karakoram Himalaya: historical perspectives on emerging threats, *Phys. Geogr.*, 31, 528–551, doi:10.2747/0272-3646.31.6.528, 2010.

Hewitt, K., Clague, J. J., and Orwin, J. F.: Legacies of catastrophic rock slope failures in mountain landscapes, *Earth-Sci. Rev.*, 87, 1–38, doi:10.1016/j.earscirev.2007.10.002, 2008.

Huber, U., Bugmann, H., and Reasoner, M. (Eds.): *Global Change and Mountain Regions. An overview of current knowledge*, in: *Advances in Global Change Research*, Vol. 23, Springer, Dordrecht, 2005.

Huggel, C.: *Assessment of Glacial Hazards based on Remote Sensing and GIS Modeling*, Dissertation, University of Zurich, Schriftenreihe Physische Geographie Glaziologie und Geomorphodynamik, 2004.

Huggel, C., Kääb, A., Haeblerli, W., Teysseire, P., and Paul, F.: Remote sensing based assessment of hazards from glacier lake outbursts: a case study in the Swiss Alps, *Can. Geotech. J.*, 39, 316–330, doi:10.1139/t01-099, 2002.

Huggel, C., Kääb, A., Haeblerli, W., and Krummenacher, B.: Regional-scale GIS-models for assessment of hazards from glacier lake outbursts: evaluation and application in the Swiss Alps, *Nat. Hazards Earth Syst. Sci.*, 3, 647–662, doi:10.5194/nhess-3-647-2003, 2003.

Huggel, C., Haeblerli, W., Kääb, A., Bieri, D. and Richardson, S.: An assessment procedure for glacial hazards in the Swiss Alps, *Can. Geotech. J.*, 41, 1068–1083, doi:10.1139/t04-053, 2004a.

Huggel, C., Kääb, A., and Salzmann, N.: GIS-based modeling of glacial hazards and their interactions using Landsat-TM and IKONOS imagery, *Norwegian Journal of Geography*, 58, 761–773, doi:10.1080/00291950410002296, 2004b.

Huggel, C., Zraggen-Oswald, S., Haeblerli, W., Kääb, A., Polkvoj, A., Galushkin, I., and Evans, S. G.: The 2002 rock/ice avalanche at Kolka/Karmadon, Russian Caucasus: assessment of extraordinary avalanche formation and mobility, and application of QuickBird satellite imagery, *Nat. Hazards Earth Syst. Sci.*, 5, 173–187, doi:10.5194/nhess-5-173-2005, 2005.

ICIMOD: *Glacial lakes and glacial lake outburst floods in Nepal*, ICIMOD, Kathmandu, 2011.

IPCC: *Climate Change 2007: The Physical Science Basis*, in: *Contribution of Working Group I to the Fourth Assessment Report of the Intergovernmental Panel on Climate Change*, edited by: Solomon, S., Qin, D., Manning, M., Chen, Z., Marquis, M., Averyt, K. B., Tignor, M., and Miller, H. L., Cambridge University Press, Cambridge and New York, 2007.

Pamir regional hazard and risk analysis

F. E. Gruber and
M. Mergili

Title Page

Abstract

Introduction

Conclusions

References

Tables

Figures

⏪

⏩

◀

▶

Back

Close

Full Screen / Esc

Printer-friendly Version

Interactive Discussion

- Iverson, R. M.: The physics of debris flows, *Rev. Geophys.*, 35, 245–296, doi:10.1029/97RG00426, 1997.
- Jarvis, A., Reuter, H. I., Nelson, A., and Guevara, E.: Hole-filled seamless SRTM data V4. International Centre for Tropical Agriculture (CIAT), available at <http://srtm.csi.cgiar.org>(last access: 19 April 2013), 2008.
- 5 Kääb, A., Huggel, C., Fischer, L., Guex, S., Paul, F., Roer, I., Salzmann, N., Schlaefli, S., Schmutz, K., Schneider, D., Strozzì, T., and Weidmann, Y.: Remote sensing of glacier- and permafrost-related hazards in high mountains: an overview, *Nat. Hazards Earth Syst. Sci.*, 5, 527–554, doi:10.5194/nhess-5-527-2005, 2005.
- 10 Kassam, K. A.: Viewing Change Through the Prism of Indigenous Human Ecology: Findings from the Afghan and Tajik Pamir, *Hum. Ecol.*, 37, 677–690, doi:10.1007/s10745-009-9284-8, 2009.
- Khromova, T. E., Osipova, G. B., Tsvetkov, D. G., Dyurgerov, M. B., and Barry, R. G.: Changes in glacier extent in the eastern Pamir, Central Asia, determined from historical data and ASTER imagery, *Remote Sens. Environ.*, 102, 24–32, doi:10.1016/j.rse.2006.01.019, 2006.
- 15 Mahmood, S. A., Shahzad, F., and Gloaguen, R.: Remote Sensing Analysis of Recent Active Tectonics in Pamir Using Digital Elevation Model: River Profile Approach, in: Proceedings of the Geoscience and Remote Sensing Symposium IGARSS, 7–11 July 2008, II-1259–II-1262, 2008.
- 20 Makhmadaliev, B., Kayumov, A., Novikov, V., Mustaeva, N., and Rajabov, I. (Eds.): The Second National Communication of the Republic of Tajikistan under the United Nations Framework Convention on Climate Change, State Agency for Hydrometeorology, Dushanbe, 2008.
- Mergili, M. and Schneider, J. F.: Regional-scale analysis of lake outburst hazards in the south-western Pamir, Tajikistan, based on remote sensing and GIS, *Nat. Hazards Earth Syst. Sci.*, 11, 1447–1462, doi:10.5194/nhess-11-1447-2011, 2011.
- 25 Mergili, M., Kopf, C., Müllebnner, B., and Schneider, J. F.: Changes of the cryosphere in the high-mountain areas of Tajikistan and Austria: a comparison, *Geogr. Ann. A*, 94, 79–96, doi:10.1111/j.1468-0459.2011.00450.x, 2012a.
- Mergili, M., Fellin, W., Moreiras, S. M., and Stötter, J.: Simulation of debris flows in the Central Andes based on Open Source GIS: Possibilities, limitations, and parameter sensitivity, *Nat. Hazards*, 61, 1051–1081, doi:10.1007/s11069-011-9965-7, 2012b.
- 30

Pamir regional hazard and risk analysis

F. E. Gruber and
M. Mergili

Title Page

Abstract

Introduction

Conclusions

References

Tables

Figures



Back

Close

Full Screen / Esc

Printer-friendly Version

Interactive Discussion

- Mergili, M., Schratz, K., Ostermann, A., and Fellin, W.: Physically-based modelling of granular flows with Open Source GIS, *Nat. Hazards Earth Syst. Sci.*, 12, 187–200, doi:10.5194/nhess-12-187-2012, 2012c.
- Mergili, M., Müller, J. P. and Schneider, J. F.: Spatio-temporal development of high-mountain lakes in the headwaters of the Amu Darya river (Central Asia), *Global Planet. Change*, in press, doi:10.1016/j.gloplacha.2013.04.001, 2013.
- Müllebnner, B.: Modelling of potential permafrost areas in the Pamir and Alai mountains (Tajikistan) using Remote Sensing and GIS techniques, Master thesis, BOKU University, Vienna, 2010.
- Narama, C., Duishonakunov, M., Kääh, A., Daiyrov, M., and Abdrakhmatov, K.: The 24 July 2008 outburst flood at the western Zyndan glacier lake and recent regional changes in glacier lakes of the Teskey Ala-Too range, Tien Shan, Kyrgyzstan, *Nat. Hazards Earth Syst. Sci.*, 10, 647–659, doi:10.5194/nhess-10-647-2010, 2010.
- Neteler, M. and Mitasova, H.: *Open source GIS: a GRASS GIS approach*, Springer, New York, 2007.
- Noetzli, J., Huggel, C., Hoelzle, M., and Haerberli, W.: GIS-based modelling of rock-ice avalanches from Alpine permafrost areas, *Computat. Geosci.*, 10, 161–178, doi:10.1007/s10596-005-9017-z, 2006.
- Quincey, D. J., Richardson, S. D., Luckman, A., Lucas, R. M., Reynolds, J. M., Hambrey, M. J., and Glasser, N. F.: Early recognition of glacial lake hazards in the Himalaya using remote sensing datasets, *Global Planet. Change*, 56, 137–152, doi:10.1016/j.gloplacha.2006.07.013, 2007.
- Risley, J. C., Walder, J. S., and Denlinger, R.: Usoi dam wave overtopping and flood routing in the Bartang and Panj rivers, Tajikistan, *Nat. Hazards*, 38, 375–390, doi:10.1007/s11069-005-1923-9, 2006.
- Richardson, S. D. and Reynolds, J. M.: An overview of glacial hazards in the Himalayas, *Quatern. Int.*, 65/66, 31–47, doi:10.1016/S1040-6182(99)00035-X, 2000.
- Rickenmann, D.: Empirical Relationships for Debris Flows, *Nat. Hazards*, 19, 47–77, doi:10.1023/A:1008064220727, 1999.
- Scheidegger, A. E.: On the Prediction of the Reach and Velocity of Catastrophic Landslides, *Rock Mech.*, 5, 231–236, doi:10.1007/BF01301796, 1973.
- Schuster, R. L. and Alford, D.: Usoi Landslide Dam and Lake Sarez, Pamir Mountains, Tajikistan, *Environ. Eng. Geosci.*, 10, 151–168, doi:10.2113/10.2.151, 2004.

Pamir regional hazard and risk analysis

F. E. Gruber and
M. Mergili

Title Page

Abstract

Introduction

Conclusions

References

Tables

Figures

⏪

⏩

◀

▶

Back

Close

Full Screen / Esc

Printer-friendly Version

Interactive Discussion

- Tinti, S., Maramai, A., and Cerutti, A. V.: The Miage Glacier in the Valley of Aosta (Western Alps, Italy) and the extraordinary detachment which occurred on August 9, 1996, *Phys. Chem. Earth Pt. A*, 24, 157–161, doi:10.1016/S1464-1895(99)00012-5, 1999.
- 5 Tweed, F. S. and Russell, A. J.: Controls on the formation and sudden drainage of glacier-impounded lakes: implications for jökulhlaup characteristics, *Prog. Phys. Geog.*, 23, 79–110, doi:10.1177/030913339902300104, 1999.
- Vilímek, V., Zapata, M. L., Klimes, J., Patzelt, Z., and Santillán, N.: Influence of glacial retreat on natural hazards of the Palcacocha Lake area, Peru, *Landslides*, 2, 107–115, doi:10.1007/s10346-005-0052-6, 2005.
- 10 Walder, J. S. and Costa, J. E.: Outburst floods from glacierdammed lakes: the effect of mode of lake drainage on flood magnitude, *Earth Surf. Proc. Land.*, 21, 701–723, doi:10.1002/(SICI)1096-9837(199608)21:8<701::AID-ESP615>3.0.CO;2-2, 1996.
- Walder, J. S. and O'Connor, J. E.: Methods for Predicting Peak Discharge of Floods Caused by Failure of Natural and Constructed Earth Dams, *Water Resour. Res.*, 33, 2337–2348, doi:10.1029/97WR01616, 1997.
- 15 Watanabe, T. and Rothacher, D.: The 1994 Lugge Tsho glacial lake outburst flood, Bhutan Himalaya, *Mt. Res. Dev.*, 16, 77–81, 1996.
- WGMS: Global Glacier Changes: Facts and Figures, edited by: Zemp, M., Roer, I., Kääb, A., Hoelzle, M., Paul, F., and Haeberli, W., UNEP, World Glacier Monitoring Service, University of Zurich, Switzerland, available at WGMS and UNEP websites: <http://www.geo.uzh.ch/microsite/wgms/> (last access: 19 April 2013) and <http://www.grid.unep.ch/glaciers/> (last access: 19 April 2013), 2008.
- 20

Pamir regional hazard and risk analysis

F. E. Gruber and
M. Mergili

Title Page

Abstract

Introduction

Conclusions

References

Tables

Figures

⏪

⏩

◀

▶

Back

Close

Full Screen / Esc

Printer-friendly Version

Interactive Discussion

Table 1. Input data, rm = raster map, tc = table column.

Parameter	Data type	Source
Elevation	rm, m a.s.l.	ASTER GDEM V2, a product of METI and NASA
Glaciers	rm, boolean	Semi-automated classification of Landsat 7 imagery
Lake ID	rm, nominal	Manual mapping from ASTER and Landsat imagery (Mergili et al., 2013)
For each lake:		
Lake type	tc, nominal	Qualitative interpretation of ASTER, Landsat and Google Earth [®] imagery (Mergili et al., 2013)
Lake drainage	tc, boolean	
Calving of ice	tc, boolean	
Lake area A_l	tc, m ²	Derived from mapped lakes
Lake evolution	tc, boolean	Mapped, 75 % confidence of growing trend in at least one of the periods 1968–2002 and 2002–2009 (Mergili et al., 2013)
Mean Annual Air Temperature (MAAT)	rm, °C	Temperature map of Müllebnner (2010) based on regression of data recorded by the Tajik HydroMet Agency with elevation
Permafrost susceptibility S_p	rm, nominal	Permafrost indication map of Mergili et al. (2012a) for Tajikistan, based on the adaptation of the rules-of-thumb of Haerberli (1975)
Seismic susceptibility S_s	rm, g	GSHAP Global Seismic Hazard Map (Giardini et al., 1999): peak ground acceleration PGA with 10 % chance of exceedance in 50 yr
Exposure E	rm, nominal	Manual mapping of land use from ASTER, Landsat
Community ID	rm, nominal	and Google Earth [®] imagery

Pamir regional hazard and risk analysis

F. E. Gruber and
M. Mergili

Table 2. Risk indication score R : combination of IH and E with scoring scheme for the exposure E as a function of land use.

$E \downarrow IH \rightarrow$	Land use	6	5	4	3	2	1	0
4 (Higher)	Built-up areas, often mixed with farmland or pastures	6	5	4	3	2	1	0
3	Farmland or pastures with some buildings	5	4	3	2	1	1	0
2	Farmland, pastures or forest with no or few buildings	4	3	2	1	1	1	0
1	Extensively used or temporarily unused land	3	2	1	1	1	1	0
0 (Lower)	No identifiable land use	0	0	0	0	0	0	0

[Title Page](#)
[Abstract](#)
[Introduction](#)
[Conclusions](#)
[References](#)
[Tables](#)
[Figures](#)




[Back](#)
[Close](#)
[Full Screen / Esc](#)
[Printer-friendly Version](#)
[Interactive Discussion](#)

Pamir regional hazard and risk analysis

F. E. Gruber and
M. Mergili

Table 3. Hazard indication score H : combination of S and M , with thresholds of (a) rock slide volume V_{rs} (10^6 m^3), (b) area of hanging glacier A_a (10^3 m^2) and (c) lake area A_l (10^3 m^2).

$M \downarrow S \rightarrow$	(a)	(b)	(c)	6	5	4	3	2	1	0
6 (Higher)	≥ 24.3	≥ 200.0	≥ 200.0	6	6	5	5	4	3	0
5	8.1– < 24.3	100.0– < 200.0	100.0– < 200.0	6	5	5	4	3	2	0
4	2.7– < 8.1	50.0– < 100.0	50.0– < 100.0	5	5	4	4	3	2	0
3	0.9– < 2.7	25.0– < 50.0	25.0– < 50.0	5	4	4	3	3	2	0
2	0.3– < 0.9	12.5– < 25.0	12.5– < 25.0	4	3	3	3	2	2	0
1	0.1– < 0.3	5.0– < 12.5	5.0– < 12.5	3	2	2	2	2	1	0
0 (Lower)	< 0.1	< 5.0	< 5.0	0	0	0	0	0	0	0

[Title Page](#)
[Abstract](#)
[Introduction](#)
[Conclusions](#)
[References](#)
[Tables](#)
[Figures](#)
[⏪](#)
[⏩](#)
[◀](#)
[▶](#)
[Back](#)
[Close](#)
[Full Screen / Esc](#)
[Printer-friendly Version](#)
[Interactive Discussion](#)


Pamir regional hazard and risk analysis

F. E. Gruber and
M. Mergili

Table 4. Impact hazard indication score IH : combination of H and I , r_{ω} is computed according to Eq. (1).

$I \downarrow H \rightarrow$	r_{ω}	6	5	4	3	2	1	0
6 (Higher)	≥ 2.000	6	6	5	5	4	3	0
5	$1.500 - < 2.000$	6	5	5	4	3	2	0
4	$1.000 - < 1.500$	5	5	4	4	3	2	0
3	$0.667 - < 1.000$	5	4	4	3	3	2	0
2	$0.333 - < 0.667$	4	3	3	3	2	2	0
1	$0.000 - < 0.333$	3	2	2	2	2	1	0
0 (Lower)	< 0.000	0	0	0	0	0	0	0

Title Page

Abstract

Introduction

Conclusions

References

Tables

Figures

⏪

⏩

◀

▶

Back

Close

Full Screen / Esc

Printer-friendly Version

Interactive Discussion



Pamir regional hazard and risk analysis

F. E. Gruber and
M. Mergili

Table 5. Rock slide susceptibility score S_{rs} . The initial values of S_{rs} are determined from the sliding plane inclination $\beta_{s,i}$, these values are then increased according to permafrost susceptibility and seismic susceptibility, g is gravity (ms^{-2}).

Criterion	Remarks	S_{rs}
Sliding plane inclination $\beta_{s,i}$	$\tan(\beta_{s,i}) \geq 1.000 - < 1.333$	1
	$\tan(\beta_{s,i}) \geq 1.333 - < 1.667$	2
	$\tan(\beta_{s,i}) \geq 1.667 - < 2.000$	3
	$\tan(\beta_{s,i}) \geq 2.000$	4
Permafrost susceptibility	No permafrost or stable permafrost	± 0
	Susceptible to melting at $\Delta\text{MAAT} > 0 - 4^\circ$	+1
Seismic susceptibility	$\text{PGA} < 0.34g$	± 0
	$\text{PGA} \geq 0.34 - < 0.65g$	+1
	$\text{PGA} \geq 0.65g$	+2

[Title Page](#)
[Abstract](#)
[Introduction](#)
[Conclusions](#)
[References](#)
[Tables](#)
[Figures](#)
[⏪](#)
[⏩](#)
[◀](#)
[▶](#)
[Back](#)
[Close](#)
[Full Screen / Esc](#)
[Printer-friendly Version](#)
[Interactive Discussion](#)

Pamir regional hazard and risk analysis

F. E. Gruber and
M. Mergili

Table 6. Scoring scheme for periglacial debris flow susceptibility S_{pf} .

Criterion	Remarks	$S_{lo,i}$
Slope β	$\tan\beta < 0.5$	0
	$\tan\beta \geq 0.5 - < 0.6$	1
	$\tan\beta \geq 0.6 - < 0.7$	2
	$\tan\beta \geq 0.7 - 0.8$	3
	$\tan\beta > 0.8$	0
Permafrost susceptibility	No permafrost or stable permafrost	0
	Susceptible to melting at $\Delta MAAT > 2 - 4^\circ$	± 0
	Susceptible to melting at $\Delta MAAT > 0 - 2^\circ$	+2
Seismic susceptibility	$PGA < 0.65g$	± 0
	$PGA \geq 0.65g$	+1

[Title Page](#)
[Abstract](#)
[Introduction](#)
[Conclusions](#)
[References](#)
[Tables](#)
[Figures](#)
[Back](#)
[Close](#)
[Full Screen / Esc](#)
[Printer-friendly Version](#)
[Interactive Discussion](#)

Pamir regional hazard and risk analysis

F. E. Gruber and
M. Mergili

Table 7. Scoring scheme for susceptibility to lake outburst triggered by internal factors S_{lo} . The initial values of S_{lo} are determined from the dam material, these values are then increased or decreased according to lake drainage, lake evolution, downstream slope of dam, permafrost susceptibility and seismic susceptibility.

Criterion	Remarks	$S_{lo,i}$
Lake type (dam material)	Erosion lake	0
	Block- or debris-dammed lake	1
	Glacial lake	3
Lake drainage	Permanent or temporary superficial drainage	-1
	No recognizable superficial drainage	± 0
Lake evolution	Stable or shrinking	± 0
	Growing trend in either the period 1968–2002 or 2002–2009	+1
Downstream slope of dam β_d	$\tan \beta_d < 0.02$	-1
	$\tan \beta_d \geq 0.02$	± 0
Permafrost susceptibility	No permafrost or stable permafrost	± 0
	Susceptible to melting at $\Delta MAAT > 0 - 4^\circ$	+1
Seismic susceptibility	PGA < 0.65 g	± 0
	PGA \geq 0.65 g	+1

[Title Page](#)
[Abstract](#)
[Introduction](#)
[Conclusions](#)
[References](#)
[Tables](#)
[Figures](#)
[Back](#)
[Close](#)
[Full Screen / Esc](#)
[Printer-friendly Version](#)
[Interactive Discussion](#)


Pamir regional hazard and risk analysis

F. E. Gruber and
M. Mergili

Table 8. Empirical relationships used for estimating the travel distance of lake outburst floods. GLOF = glacial lake outburst flood, L = travel distance, V_d = debris flow volume, ΔZ = loss of elevation, ω_r = average slope of reach, Q_p = peak discharge.

	Relationship	References	Remarks
T1	$L = 1.9V_d^{0.16} \Delta Z^{0.83}$	Rickenmann (1999)	for debris flows in general
T2	$\omega_r = 11^\circ$	Haeberli (1983), Huggel et al. (2003, 2004a)	for debris flows from GLOFs, applied with $\omega_r = 8^\circ$ in the present study (Mergili and Schneider, 2011)
T3	$\omega_r = 18Q_p^{-0.07}$	Huggel (2004)	worst case for debris flows from GLOFs
T4	$\omega_r \geq 2^\circ$	Haeberli (1983), Huggel et al. (2004a)	for floods from GLOFs

[Title Page](#)
[Abstract](#)
[Introduction](#)
[Conclusions](#)
[References](#)
[Tables](#)
[Figures](#)
[⏪](#)
[⏩](#)
[◀](#)
[▶](#)
[Back](#)
[Close](#)
[Full Screen / Esc](#)
[Printer-friendly Version](#)
[Interactive Discussion](#)

Pamir regional hazard and risk analysis

F. E. Gruber and
M. Mergili

Table 9. Empirical regression equations relating peak discharge Q_p of glacial lakes to outburst volume V_l and lake depth (dam height) D_l . ρ_w = density of water (kg m^{-3}), g = gravity (ms^{-2}), * envelope (worst case).

Reference		Q_p ($\text{m}^3 \text{s}^{-1}$) of glacial lakes
Costa (1985)	Q1	$113 \left(10^{-6} V_l\right)^{0.61}$
	Q2	$3.8 \left(10^{-6} V_l D_l\right)^{0.61}$
Costa and Schuster (1988)	Q3	$1.3 \times 10^{-4} (\rho_w g V_l D_l)^{0.60}$
	Q4	$5.5 \times 10^{-6} (\rho_w g V_l D_l)^{0.59}$
Walder and O'Connor (1997)	Q5*	$2.2 \times 10^{-1} V_l^{0.66}$
	Q6*	$1.1 (V_l D_l)^{0.47}$

[Title Page](#)
[Abstract](#)
[Introduction](#)
[Conclusions](#)
[References](#)
[Tables](#)
[Figures](#)
[Back](#)
[Close](#)
[Full Screen / Esc](#)
[Printer-friendly Version](#)
[Interactive Discussion](#)

Pamir regional hazard and risk analysis

F. E. Gruber and
M. Mergili

Title Page

Abstract

Introduction

Conclusions

References

Tables

Figures

◀

▶

◀

▶

Back

Close

Full Screen / Esc

Printer-friendly Version

Interactive Discussion

Table 10. Percentage of lakes assigned each class of lake outburst (LO) susceptibility (internal and external factors) and hazard indication scores according to lake type.

Lake type	LO susceptibility score (internal factors)							Sum
	0	1	2	3	4	5	6	
Erosion lakes	33.1%	40.8%	24.7%	1.5%	0.0%	0.0%	0.0%	883
Block- or debris-dammed lakes	12.4%	17.1%	44.8%	24.8%	1.0%	0.0%	0.0%	105
Glacial lakes	38.2%	0.0%	0.0%	4.4%	31.1%	24.5%	1.7%	652
Lake type	LO susceptibility score (external factors)							Sum
	0	1	2	3	4	5	6	
Erosion lakes	42.1%	5.3%	18.9%	16.5%	7.5%	7.7%	1.9%	883
Block- or debris-dammed lakes	18.1%	1.0%	10.5%	14.3%	18.1%	32.4%	5.7%	105
Glacial lakes	40.8%	0.2%	3.5%	11.3%	15.5%	21.3%	7.4%	652
Lake type	LO hazard indication score							Sum
	0	1	2	3	4	5	6	
Erosion lakes	24.5%	5.8%	34.2%	19.0%	10.6%	5.3%	0.6%	883
Block- or debris-dammed lakes	12.4%	0.0%	31.4%	23.8%	13.3%	16.2%	2.9%	105
Glacial lakes	38.2%	0.0%	26.5%	20.2%	10.4%	4.4%	0.2%	652

Pamir regional hazard and risk analysis

F. E. Gruber and
M. Mergili

Title Page

Abstract

Introduction

Conclusions

References

Tables

Figures



Back

Close

Full Screen / Esc

Printer-friendly Version

Interactive Discussion



Table 12. Per cent of communities assigned to each class of the community risk indication score. RS = rock slides, IA = ice avalanches, PF = periglacial debris flows, LO = lake outburst floods.

Process type	Community risk indication score						
	0	1	2	3	4	5	6
RS	12.1 %	9.7 %	8.6 %	15.3 %	27.5 %	23.9 %	2.9 %
IA	75.2 %	8.9 %	5.7 %	4.8 %	2.2 %	2.4 %	0.8 %
PF	11.5 %	3.7 %	6.1 %	9.2 %	24.4 %	31.4 %	13.9 %
LO	65.6 %	12.3 %	11.6 %	6.2 %	2.9 %	1.4 %	0.0 %

Pamir regional hazard and risk analysis

F. E. Gruber and
M. Mergili

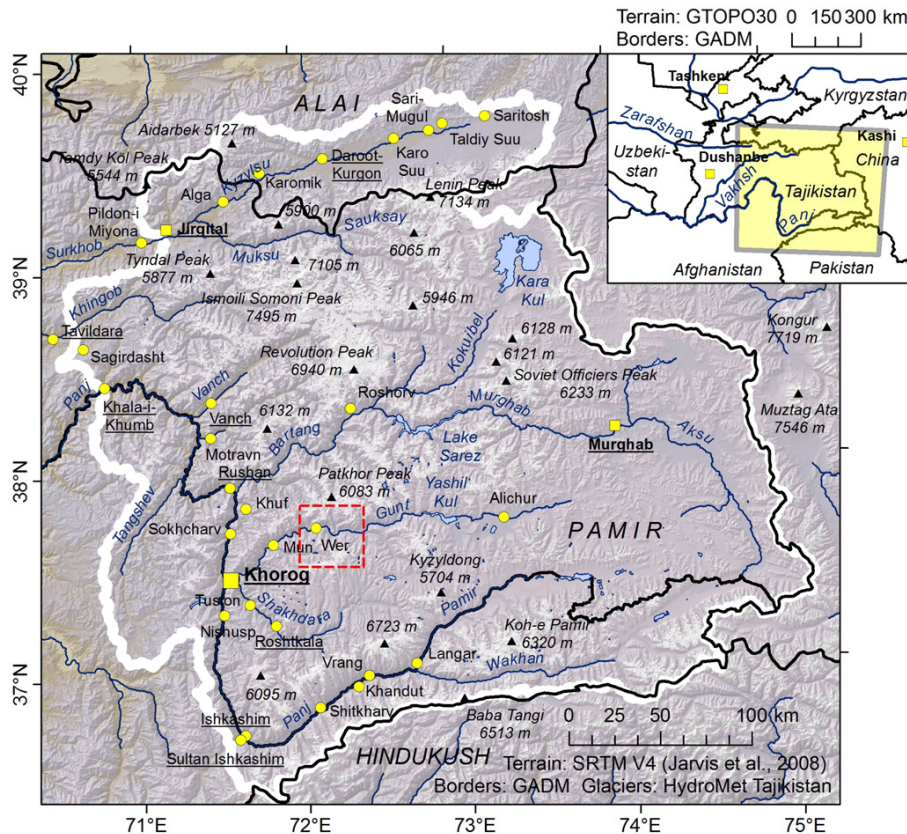


Fig. 1. Study area. The dashed red rectangle delimits the area shown in Fig. 14.

Title Page

Abstract

Introduction

Conclusions

References

Tables

Figures



Back

Close

Full Screen / Esc

Printer-friendly Version

Interactive Discussion



Pamir regional hazard and risk analysis

F. E. Gruber and
M. Mergili

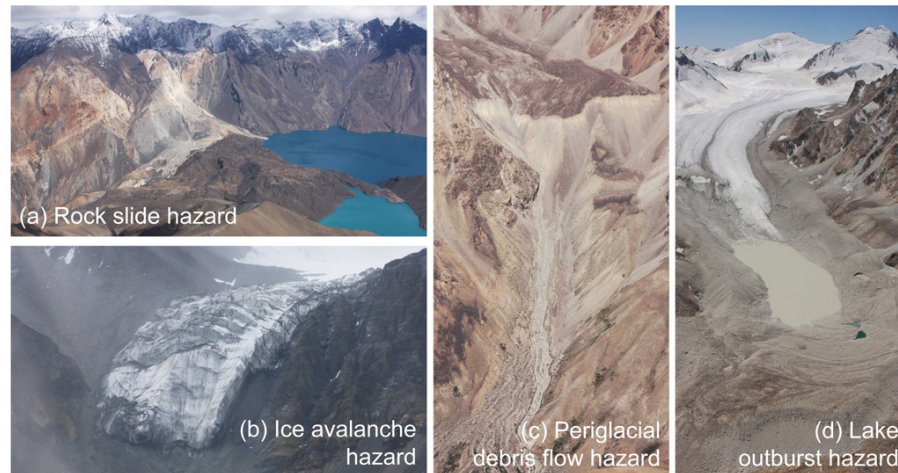


Fig. 2. Processes covered by the high-mountain multi-hazard and -risk indication model. **(a)** The 2 km² rock slide deposit impounding lake Sarez, triggered by an earthquake in 2011, **(b)** hanging glacier in the Sauksay Valley prone to produce ice avalanches, **(c)** periglacial debris flow starting from a rock glacier terminus in the upper Gunt Valley, and **(d)** Lake Varshedz in a southern tributary of the Gunt Valley, one of many glacial lakes possibly susceptible to sudden drainage. All photos taken by M. Mergili.

[Title Page](#)
[Abstract](#)
[Introduction](#)
[Conclusions](#)
[References](#)
[Tables](#)
[Figures](#)
[⏪](#)
[⏩](#)
[◀](#)
[▶](#)
[Back](#)
[Close](#)
[Full Screen / Esc](#)
[Printer-friendly Version](#)
[Interactive Discussion](#)


Pamir regional hazard and risk analysis

F. E. Gruber and
M. Mergili

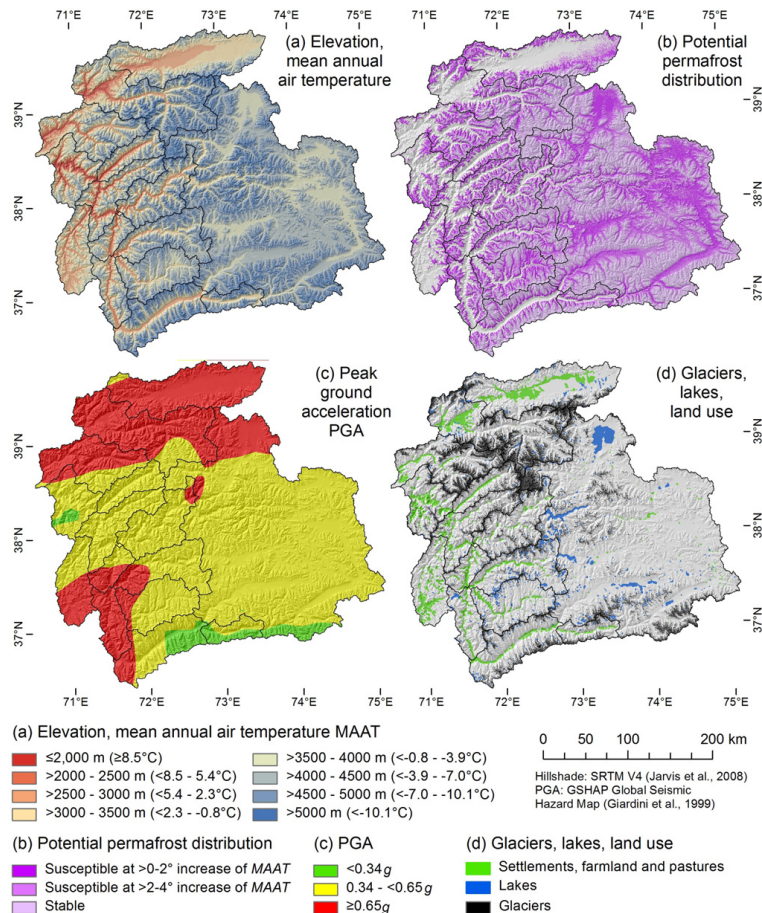


Fig. 3. Input data: **(a)** elevation and mean annual air temperature, **(b)** potential permafrost distribution, **(c)** peak ground acceleration, and **(d)** mapped glaciers, lakes and land use.

Title Page

Abstract Introduction

Conclusions References

Tables Figures

◀ ▶

◀ ▶

Back Close

Full Screen / Esc

Printer-friendly Version

Interactive Discussion

Pamir regional hazard and risk analysis

F. E. Gruber and M. Mergili

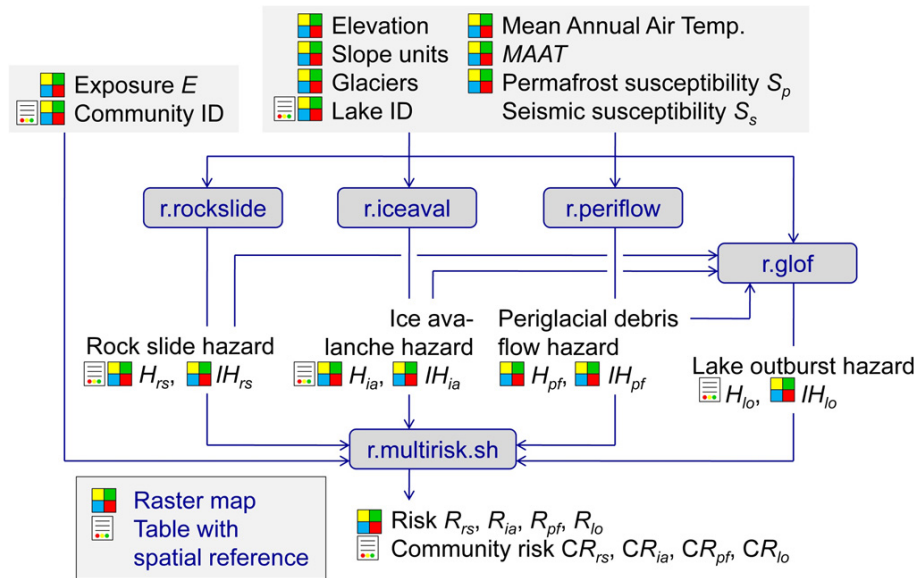


Fig. 4. Logical framework of the high-mountain multi-hazard and -risk indication model.

Discussion Paper | Discussion Paper | Discussion Paper | Discussion Paper | Discussion Paper

Title Page

Abstract Introduction

Conclusions References

Tables Figures

⏪ ⏩

◀ ▶

Back Close

Full Screen / Esc

Printer-friendly Version

Interactive Discussion



Pamir regional hazard and risk analysis

F. E. Gruber and
M. Mergili

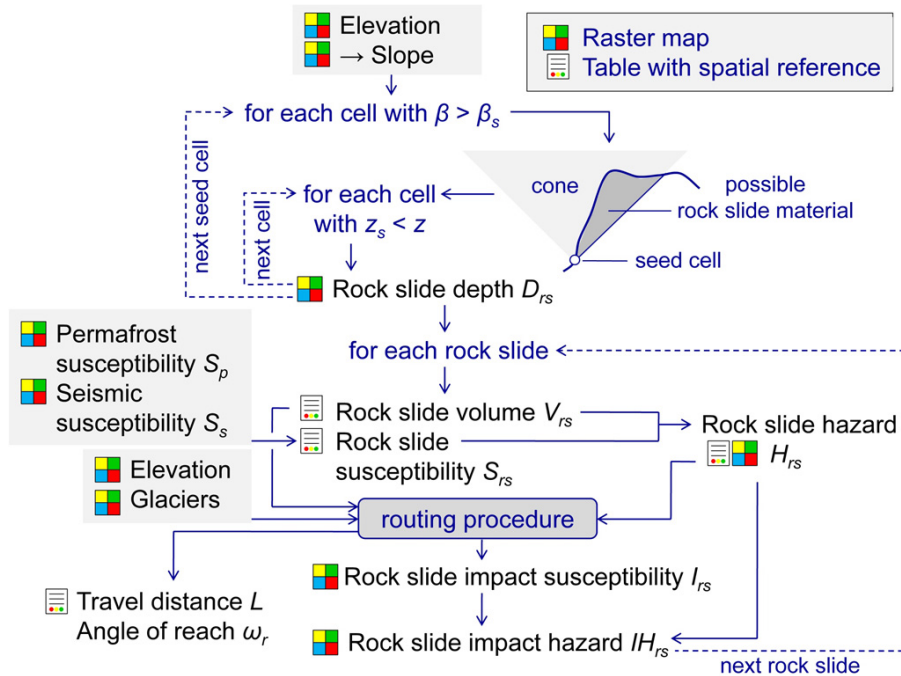


Fig. 5. Logical framework of the rock slide model (r.rockslide).

Title Page

Abstract

Introduction

Conclusions

References

Tables

Figures

⏪

⏩

◀

▶

Back

Close

Full Screen / Esc

Printer-friendly Version

Interactive Discussion

Pamir regional hazard and risk analysis

F. E. Gruber and
M. Mergili

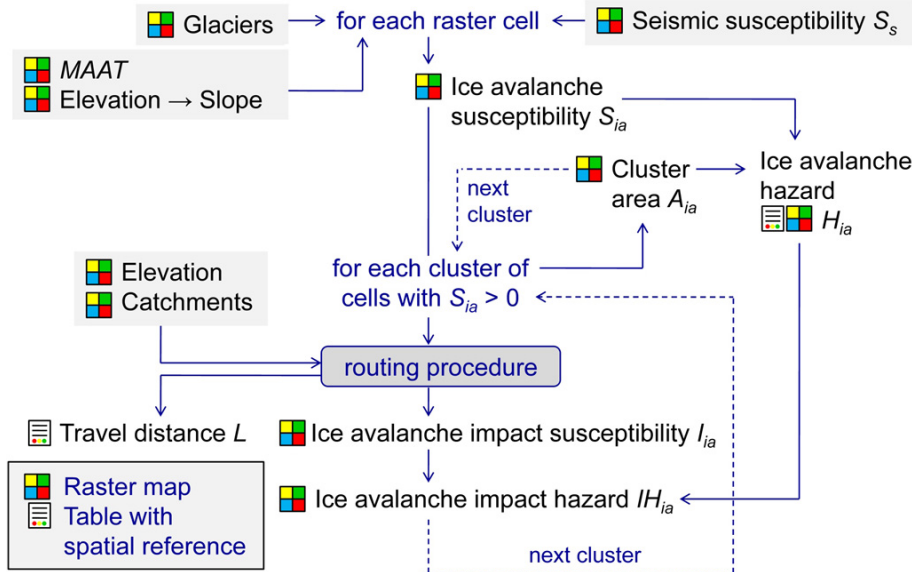


Fig. 6. Logical framework of the ice avalanche model (r.iceaval).

Title Page	
Abstract	Introduction
Conclusions	References
Tables	Figures
◀	▶
◀	▶
Back	Close
Full Screen / Esc	
Printer-friendly Version	
Interactive Discussion	

Pamir regional hazard and risk analysis

F. E. Gruber and
M. Mergili

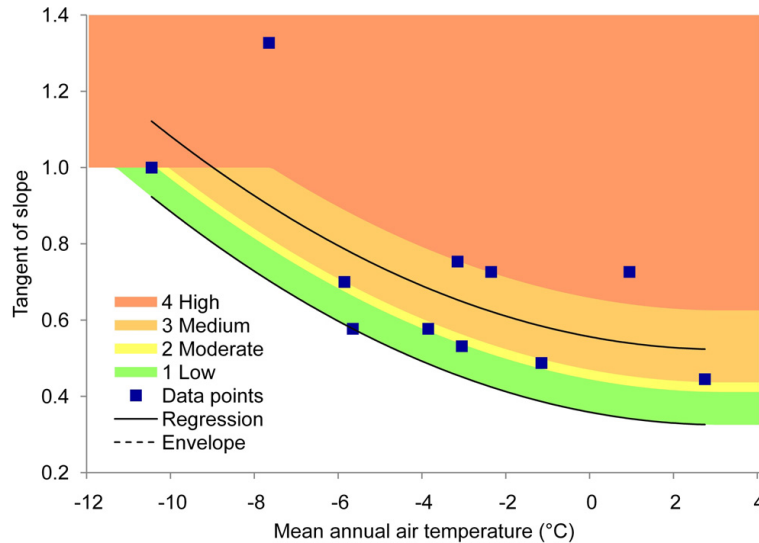


Fig. 7. Scoring scheme applied for ice avalanche susceptibility according to data presented by Alean (1985) and Huggel et al. (2004a).

Title Page

Abstract

Introduction

Conclusions

References

Tables

Figures

⏪

⏩

◀

▶

Back

Close

Full Screen / Esc

Printer-friendly Version

Interactive Discussion



Pamir regional hazard and risk analysis

F. E. Gruber and
M. Mergili

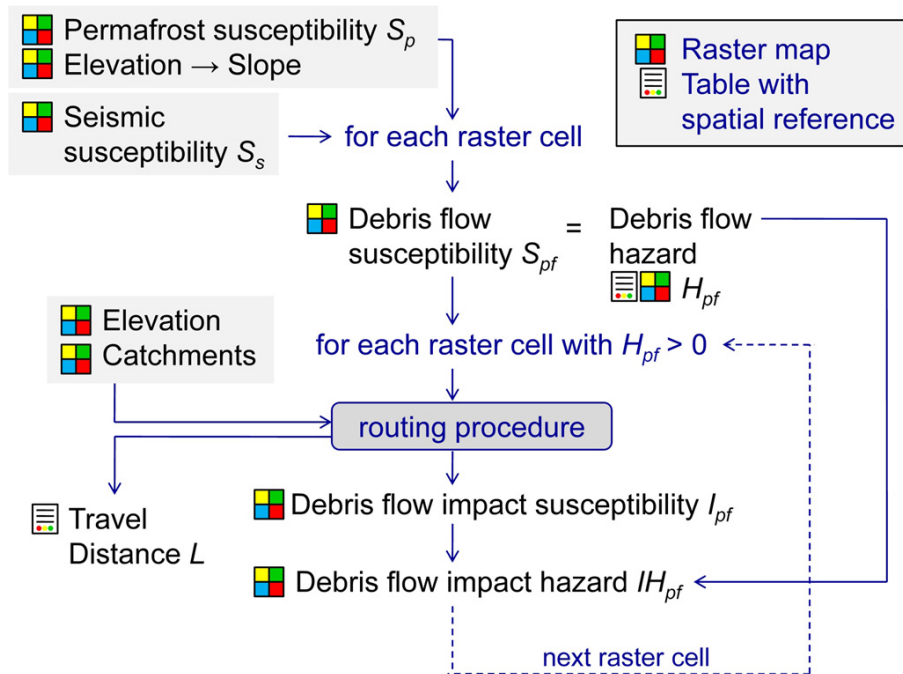


Fig. 8. Logical framework of the periglacial debris flow model (r.periflow).

Title Page	
Abstract	Introduction
Conclusions	References
Tables	Figures
◀	▶
◀	▶
Back	Close
Full Screen / Esc	
Printer-friendly Version	
Interactive Discussion	

Pamir regional hazard and risk analysis

F. E. Gruber and M. Mergili

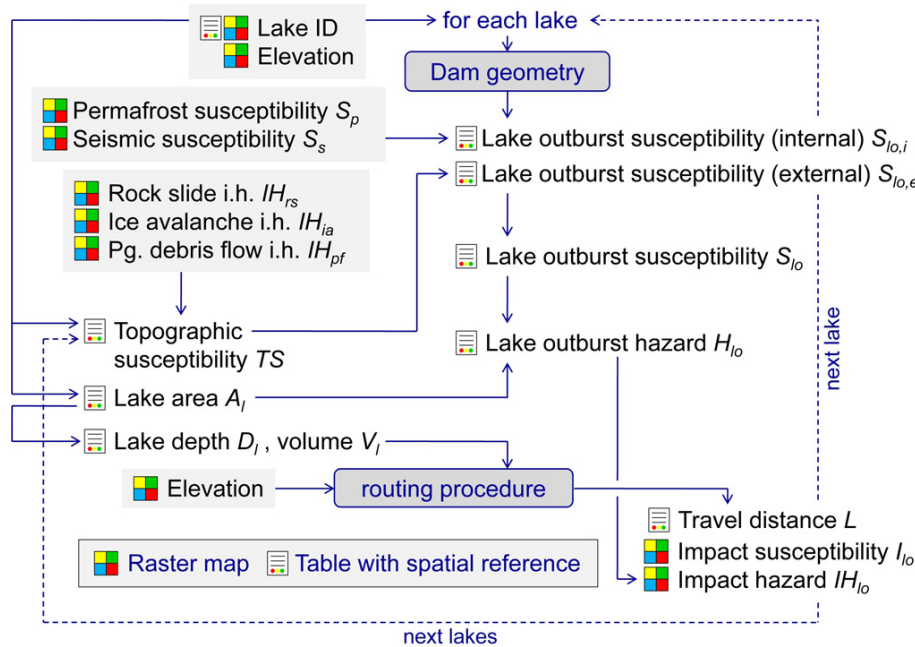


Fig. 9. Logical framework of the lake outburst model (r.glof).

Title Page

Abstract Introduction

Conclusions References

Tables Figures

⏪ ⏩

◀ ▶

Back Close

Full Screen / Esc

Printer-friendly Version

Interactive Discussion



Pamir regional hazard and risk analysis

F. E. Gruber and
M. Mergili

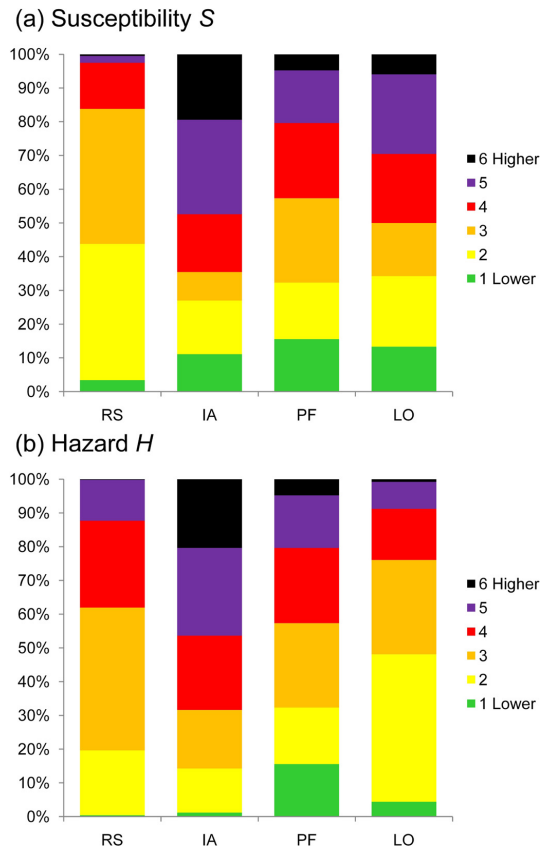


Fig. 10. Relative abundance of **(a)** the susceptibility and **(b)** the hazard indication score values for the four considered processes. The values for rock slides (RS), ice avalanches (IA) and periglacial debris flows (PF) relate to raster cells, the values for lake outburst floods (LO) to lakes. Only those raster cells or lakes with a score of at least 1 are considered.

Title Page	
Abstract	Introduction
Conclusions	References
Tables	Figures
⏪	⏩
◀	▶
Back	Close
Full Screen / Esc	
Printer-friendly Version	
Interactive Discussion	



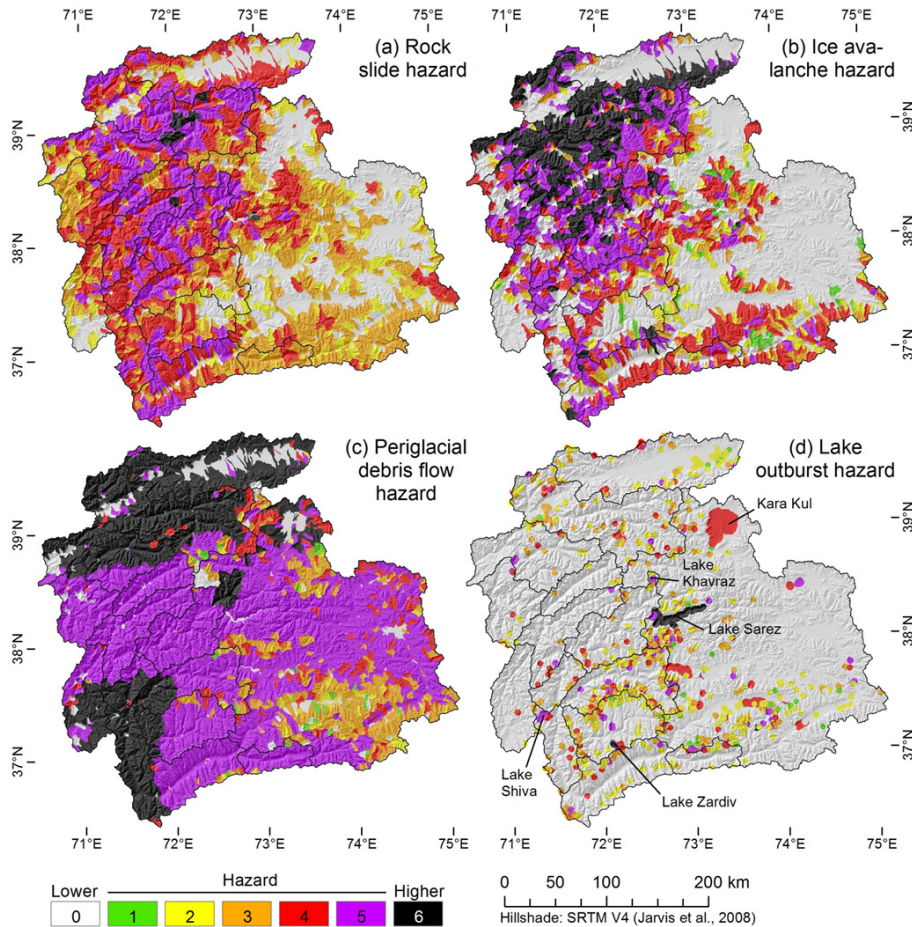


Fig. 11. Distribution of **(a)** rock slide, **(b)** ice avalanche, **(c)** periglacial debris flow, and **(d)** lake outburst hazard over the entire study area. The maximum score is shown for each catchment.

Pamir regional hazard and risk analysis

F. E. Gruber and M. Mergili

Title Page

Abstract Introduction

Conclusions References

Tables Figures

◀ ▶

◀ ▶

Back Close

Full Screen / Esc

Printer-friendly Version

Interactive Discussion



Pamir regional hazard and risk analysis

F. E. Gruber and
M. Mergili

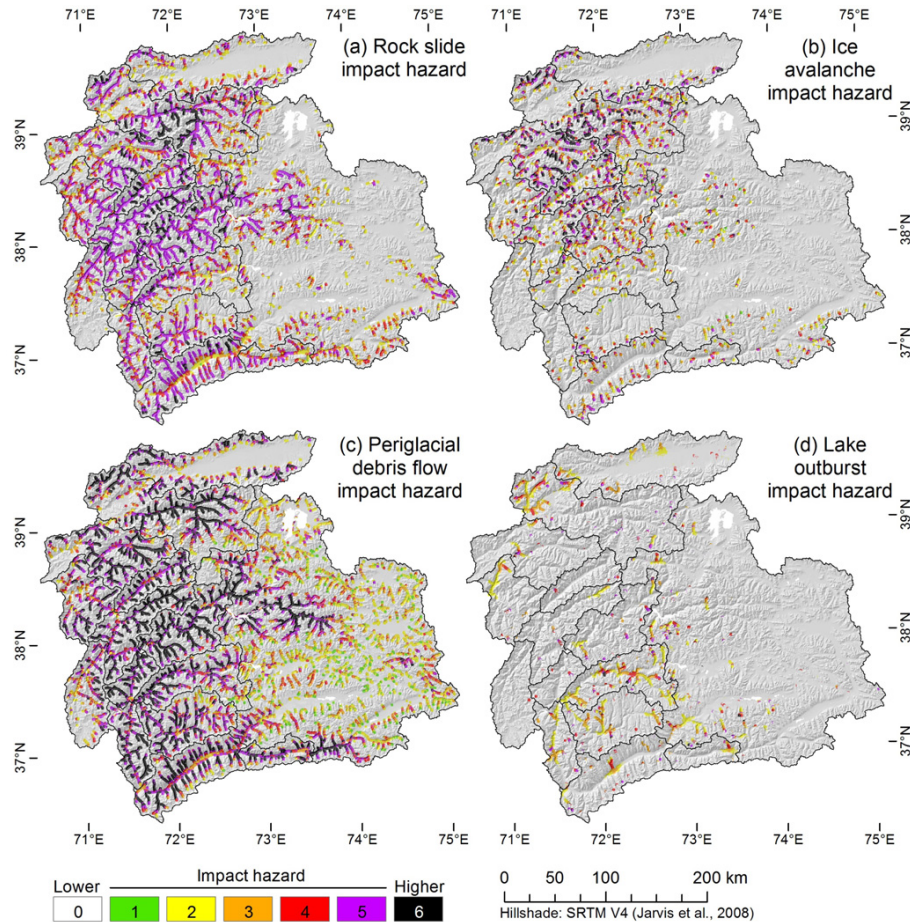


Fig. 12. Impact hazard for each process, **(a)** rock slides, **(b)** ice avalanches, **(c)** periglacial debris flows, and **(d)** lake outburst floods. For clarity, only the scores along the main flow lines are shown.

[Title Page](#)
[Abstract](#)
[Introduction](#)
[Conclusions](#)
[References](#)
[Tables](#)
[Figures](#)
[⏪](#)
[⏩](#)
[◀](#)
[▶](#)
[Back](#)
[Close](#)
[Full Screen / Esc](#)
[Printer-friendly Version](#)
[Interactive Discussion](#)

Pamir regional hazard and risk analysis

F. E. Gruber and
M. Mergili

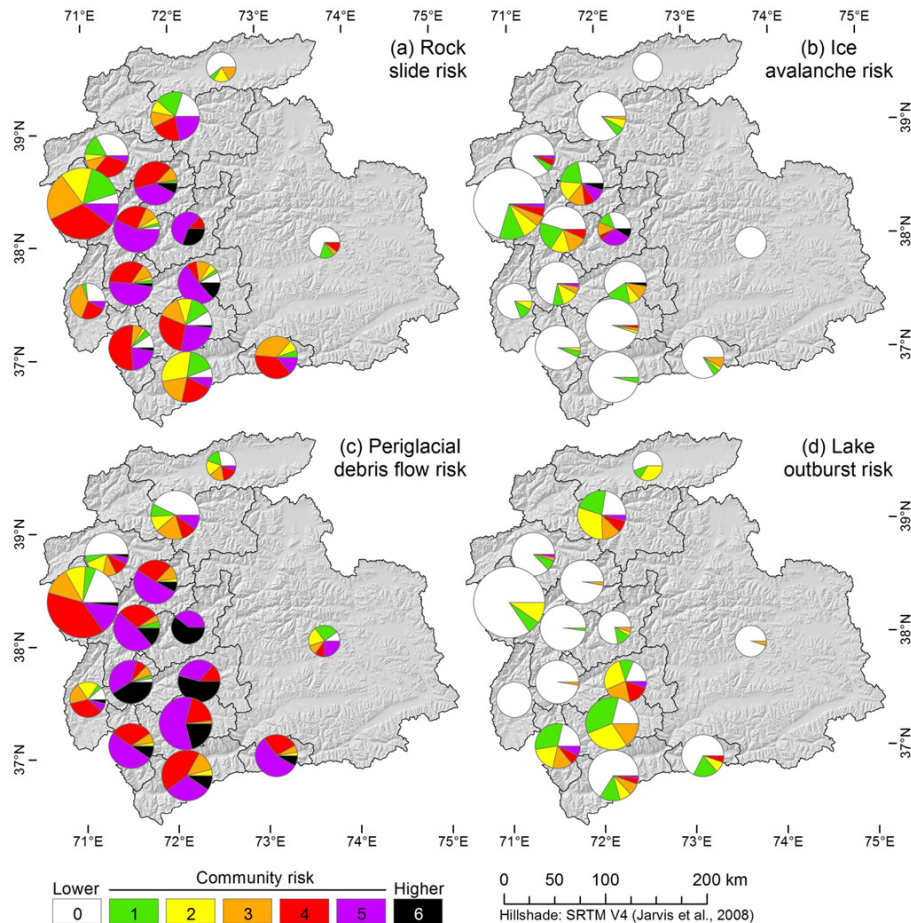


Fig. 13. Community risk, generalized to 15 regions. For each region, the pie chart illustrates the relative abundance of the different community risk indication scores. The size of each chart is proportional to the number of communities it represents.

Pamir regional hazard and risk analysis

F. E. Gruber and M. Mergili

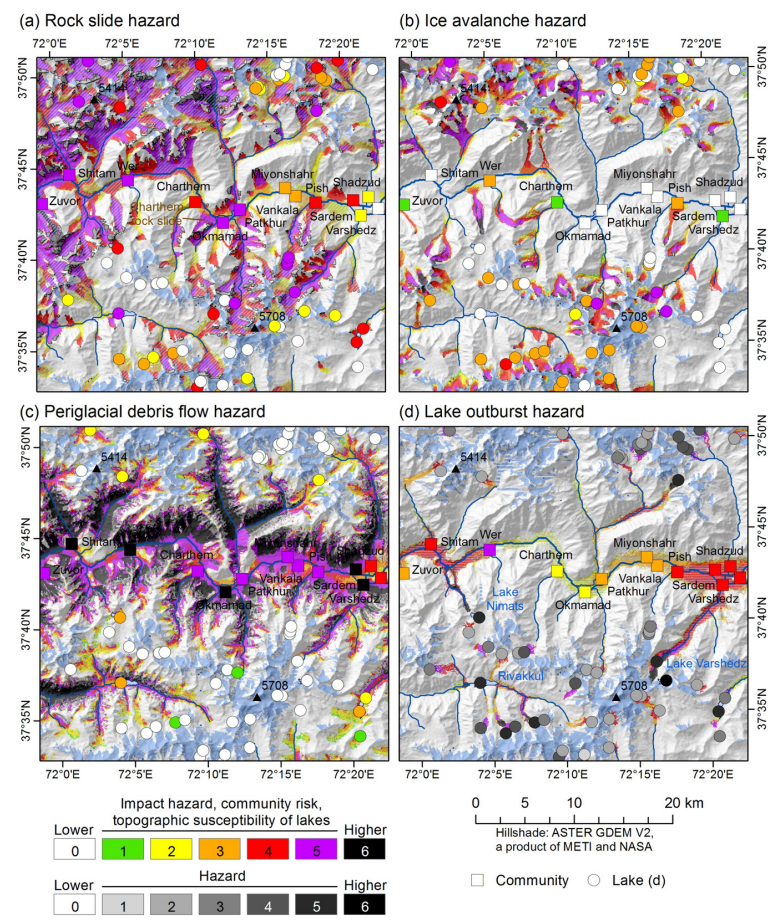


Fig. 14. Hazard, impact hazard, topographic susceptibility of lakes and community risk associated with each process type. **(a)** Rock slide, **(b)** ice avalanche, **(c)** periglacial debris flow, and **(d)** lake outburst flood. The extent of the map is shown in Fig. 1.

Title Page

Abstract Introduction

Conclusions References

Tables Figures

⏪ ⏩

◀ ▶

Back Close

Full Screen / Esc

Printer-friendly Version

Interactive Discussion

